Published OnlineFirst December 15, 2014; DOI: 10.1158/1535-7163.MCT-14-0765

Small Molecule Therapeutics

Molecular Cancer Therapeutics

Identification of Novel Radiosensitizers in a High-Throughput, Cell-Based Screen for DSB Repair Inhibitors

Alexander G. Goglia[1], Robert Delsite[1], Antonio N. Luz[2], David Shahbazian[3], Ahmed F. Salem[4], Ranjini K. Sundaram[4], Jeanne Chiaravalli[2], Petrus J. Hendrikx[5], Jennifer A. Wilshire[5], Maria Jasin[6], Harriet M. Kluger[3], J. Fraser Glickman[2], Simon N. Powell[1], and Ranjit S. Bindra[4]

Abstract

Most cancer therapies involve a component of treatment that inflicts DNA damage in tumor cells, such as double-strand breaks (DSBs), which are considered the most serious threat to genomic integrity. Complex systems have evolved to repair these lesions, and successful DSB repair is essential for tumor cell survival after exposure to ionizing radiation (IR) and other DNA-damaging agents. As such, inhibition of DNA repair is a potentially efficacious strategy for chemo- and radiosensitization. Homologous recombination (HR) and nonhomologous end-joining (NHEJ) represent the two major pathways by which DSBs are repaired in mammalian cells. Here, we report the design and execution of a high-throughput, cell-based small molecule screen for novel DSB repair inhibitors. We miniaturized our recently developed dual NHEJ and HR reporter system into a 384-well plate-based format and interrogated a diverse library of 20,000 compounds for molecules that selectively modulate NHEJ and HR repair in tumor cells. We identified a collection of novel hits that potently inhibit DSB repair, and we have validated their functional activity in a comprehensive panel of orthogonal secondary assays. A selection of these inhibitors was found to radiosensitize cancer cell lines *in vitro*, which suggests that they may be useful as novel chemo- and radio sensitizers. Surprisingly, we identified several FDA-approved drugs, including the calcium channel blocker mibefradil dihydrochloride, that demonstrated activity as DSB repair inhibitors and radiosensitizers. These findings suggest the possibility for repurposing them as tumor cell radiosensitizers in the future. Accordingly, we recently initiated a phase I clinical trial testing mibefradil as a glioma radiosensitizer. *Mol Cancer Ther; 14(2); 326–42. ©2014 AACR.*

Introduction

Most cancer therapies involve a component of treatment that inflicts DNA damage in tumor cells. Ionizing radiation (IR) is a potent inducer of double-strand breaks (DSB), which are considered the most serious form of DNA damage. Complex systems have evolved to rapidly detect and repair these lesions, and successful DSB repair is essential for tumor cell survival after exposure to IR and other DNA-damaging agents. Homologous recombination (HR) and nonhomologous end-joining (NHEJ) represent the two major DSB repair pathways in cells (1–4). Emerging evidence suggests that inhibition of DNA repair and damage checkpoints is a viable and potentially efficacious strategy for chemo- and radiosensitization in the clinic, which has been supported by decades of work confirming a link between DNA repair and tumor cell survival after IR (5). Examples of such drugs in clinical trials and/or active preclinical development include inhibitors of poly (ADP-ribose) polymerase (PARP; ref. 6), checkpoint kinase 1 and 2 (Chk1 and Chk2; ref. 7), and DNA-dependent protein kinase (DNA-PK; ref. 8). Most of these drugs were identified in high-throughput screens using a target-based, "reverse chemical genetics" strategy focused on these particular targets (9). In this approach, a small molecule library is screened for compounds that bind or inhibit a particular protein of interest, typically using *in vitro* assays with purified proteins. However, there are numerous steps in key DSB repair pathways that have not yet been targeted. These findings suggest the need for additional efforts, and also alternative drug screening strategies, to identify new drugs that can inhibit DSB repair. Here, we report on the results of a high-throughput, cell-based screen for novel inhibitors of NHEJ and HR repair, using a forward chemical genetics approach.

The HR pathway uses homologous DNA sequences as a template for repair, whereas NHEJ processes and re-ligates the ends of the breaks (10). NHEJ repair is considered more error prone than HR and occurs more frequently in cells. NHEJ is the predominant pathway in the G_0–G_1-phases of the cell cycle, whereas HR increases during S-phase, when a sister chromatid becomes

[1]Department of Radiation Oncology, Memorial Sloan Kettering Cancer Center, New York, New York. [2]High Throughput and Spectroscopy Resource Center, Rockefeller University, New York, New York. [3]Section of Medical Oncology, Yale Cancer Center, Yale University School of Medicine, New Haven, Connecticut. [4]Department of Therapeutic Radiology, Yale University School of Medicine, New Haven, Connecticut. [5]Flow Cytometry Core Facility, Memorial Sloan Kettering Cancer Center, New York, New York. [6]Developmental Biology Program, Memorial Sloan Kettering Cancer Center, New York, New York.

Note: Supplementary data for this article are available at Molecular Cancer Therapeutics Online (http://mct.aacrjournals.org/).

Corresponding Authors: Ranjit S. Bindra, Department of Therapeutic Radiology, Yale University School of Medicine, 333 Cedar Street, New Haven, CT 06520. Phone: 203-584-0924; Fax: 203-200-3673; E-mail: ranjit.bindra@yale.edu; and Simon N. Powell, Department of Radiation Oncology, Memorial Sloan Kettering Cancer Center, 1275 York Avenue, New York, NY 10065. E-mail: powells@mskcc.org

doi: 10.1158/1535-7163.MCT-14-0765

Published OnlineFirst December 15, 2014; DOI: 10.1158/1535-7163.MCT-14-0765

available as a template for repair. As cells enter the G_2–M-phase of the cell cycle, NHEJ becomes more active and likely predominates over HR repair (11). Emerging evidence indicates that many subpathways exist within both the NHEJ and HR pathways of repair. In particular, NHEJ repair mainly is composed of canonical NHEJ (cNHEJ) and noncanonical NHEJ repair. The latter process has been given many names, including back-up NHEJ (bNHEJ), alternative NHEJ (aNHEJ), and microhomology-mediated NHEJ (MMEJ; ref. 12). This lack of consensus, in part, can be attributed to the fact that specific DSB repair proteins that mediate noncanonical NHEJ repair remain elusive. The cNHEJ pathway is well defined and results in minimal processing of the DSB ends (13), while the latter process typically results in deletions with local sequence microhomology (14–17). cNHEJ proteins include Ku70/80, DNA-PK catalytic subunit (DNA-PKcs), X-ray repair cross-complementing protein 4 (XRCC4), and ligase IV (13). As noted above, the noncanonical pathway(s) are poorly defined but appear to require MRE11 (18) and PARP-1 (19). Ligase III and X-ray repair cross-complementing protein 1 (XRCC1) are also implicated in these processes (20, 21), although more recent studies have questioned the requirement of these proteins (22–24). Examples of key HR proteins include breast cancer 1 (BRCA1), BRCA2, and Rad51 (10). CtIP is a key HR factor involved in the initial end-resection step of this process (25), but it also appears to play a role in NHEJ repair, particularly in pathways distinct from cNHEJ (26). Collectively, the noncanonical NHEJ repair processes share a common theme of higher rates of insertions, deletions, and microhomology usage. As such, we have termed this pathway mutagenic NHEJ (mNHEJ) repair previously, to distinguish cNHEJ repair versus bNHEJ, aNHEJ, MMEJ, which often are used interchangeably but sometimes distinctly (27). However, MMEJ repair specifically may represent a subset of mNHEJ in which flanking sequence microhomology is commonly (if not exclusively) used. Another DSB repair pathway has been described, single-strand annealing (SSA), which is distinct from NHEJ repair and likely represents a subpathway of HR repair. SSA repair anneals adjacent sequence repeats flanking a DSB, resulting in a deletion between the repeats (28).

Numerous assays to measure DSB repair in cells have been described previously, and they typically use IR or endonucleases to induce DNA cleavage events at chromosomal loci or in plasmid substrates. DSB repair proteins form discrete foci at DNA damage sites after treatment with IR, which can be visualized by immunofluorescence microscopy. These foci patterns can be used as markers for DSB repair in cultured cells (29, 30). DSB repair can also be assayed using the neutral comet assay, which relies on the altered mobility of cleaved DNA (31). Weingeist and colleagues (32) recently demonstrated that this technique can be miniaturized for high-throughput screening. Fluorescence-based assays also have become an important tool to assess DSB repair in cells. The DR-GFP assay is a commonly used HR assay, which uses the I-SceI endonuclease to induce a site-specific DSB in a cell (33). We recently developed a novel mNHEJ repair assay, termed end joining-red fluorescent protein (EJ-RFP), which can be combined with DR-GFP to measure both DSB repair pathways simultaneously (27). We integrated this system into a number of cells, including U2OS DR-GFP cells (referred to as U2OS EJ-DR cells). We also developed a novel, ligand-dependent I-SceI system for DSB induction in cells (27). A similar inducible I-SceI system subsequently was described by Truong and colleagues (34). Many other elegant reporter assays and inducible cleavage systems have been described previously, which have been used to gain critical insights into DSB repair regulation (15, 18), (35–38).

Here, we report the design and execution of a high-throughput, cell-based small molecule screen for novel DSB repair inhibitors. We miniaturized our recently developed dual mNHEJ and HR reporter system into a 384-well plate-based format, and we then interrogated a diverse library of approximately 20,000 compounds for molecules that selectively modulate mNHEJ and/or HR repair in tumor cells. We identified a collection of novel hits that potently inhibit DSB repair, and we validated their functional activity in a comprehensive panel of orthogonal secondary assays. A selection of these inhibitors was found to radiosensitize cancer cell lines *in vitro*, which suggests they may be useful as novel chemo- and radiosensitizers for solid tumors in which local recurrence after therapy is a barrier to treatment efficacy. Surprisingly, we identified several currently or previously FDA-approved drugs, including the calcium channel blocker, mibefradil dihydrochloride, which demonstrated substantial activity as DSB repair inhibitors and radiosensitizers. These findings suggest the possibility for repurposing them as tumor cell radiosensitizers in the future. Along these lines, we recently initiated a phase I clinical trial testing mibefradil as a radiosensitizer in patients with recurrent glioblastoma.

Materials and Methods

Cell lines and culture conditions

U2OS EJ-DRs, which consist of the U2OS osteosarcoma cell line with integrated copies of the EJ-RFP and DR-GFP reporters, along with the ligand-inducible ddSceGR cleavage system, have been described previously (27). The parental U2OS cell line and T98G cells were obtained directly from the American Type Culture Collection (ATCC), which has provided certification of authentication per the guidelines that are published on their website (i.e., using STR Profiling Analysis). Additional U2OS cells lines containing the GFP-based DSB repair assays to measure SSA, total NHEJ, and MMEJ were a generous gift from Jeremy Stark (Department of Radiation Biology, Beckman Research Institute of City of Hope) and have been described and validated for authenticity previously (35, 36). These cell lines were cultured in high-glucose Dulbecco's Modified Eagle Medium (DMEM) with L-glutamine containing 10% tetracycline-free (tet-free) fetal bovine serum (FBS; Clontech Laboratories and Atlanta Biologics). All cells were maintained at 37°C with 5% CO_2. Tet-free serum, instead of "regular" FBS, is needed for routine passaging during experiments involving U2OS EJ-DRs cells, to prevent *DsRed* gene expression in the EJ-RFP system, which can result from residual tetracycline found in most commercially available FBS preparations. For the long-term culture of U2OS EJ-DRs cells, we used charcoal-stripped FBS (Invitrogen Corporation), to minimize the levels of endogenous glucocorticoids present in untreated FBS preparations. Ligand-induced DNA cleavage by ddSceGR was performed by adding the Shield1 and triamcinolone acetonide ligands at concentrations of 0.5 to 1 μmol/L and 100 nmol/L, respectively, to the cell cultures. Ligands were incubated in the cells for 24 hours, followed by one or two washes with DMEM containing 10% FBS without ligands. Specific conditions for ligand addition in microplates are described below. All control drugs presented in this study were purchased from Tocris Bioscience.

Published OnlineFirst December 15, 2014; DOI: 10.1158/1535-7163.MCT-14-0765

High-throughput small molecule screening

All primary drug screening studies were performed in polystyrene clear bottom black-walled 384-well microplates (Greiner Bio One International AG). The process for DSB induction, cell incubation, and timing of reporter gene measurement using the EJ-DRs assay was described in detail previously (27). All screening compounds and control drugs were added from 5 mmol/L source plates in DMSO directly to microplates containing 10 μL of DMEM without FBS (referred to as "preplating"), such that the final concentration was 10 μmol/L, and used within 24 hours of compound/drug dilution. The test compounds were dispensed with Norgren Kloehn nanosyringes and each plate was bar-coded for tracking at the Rockefeller High-Throughput & Spectroscopy Resource Center (HTSRC; New York, NY), using well-established in-house protocols at this facility. The control drugs were added manually with a multichannel pipettor for the initial screening optimization studies with known DSB repair inhibitors. DMSO alone (1%) was added to columns 23 and 24 for all microplates unless otherwise specified below in the Results (and these columns were reserved for negative and positive controls, as described below). U2OS EJ-DRs cells were seeded into each well at a final concentration of 1,000 cells per well, in a volume of 40 μL containing 12.5% tet-free FBS, such that the final FBS concentration was 10% v/v in each microplate well. This media also contained the DSB ligands, Shield1 and triamcinolone acetonide, which yielded final concentrations of 1 μmol/L and 100 nmol/L, respectively. The media for column 24 in each plate *did not* contain these DSB ligands, which served as the equivalent of a *positive control* representing maximal inhibition of mNHEJ and HR repair. Phenol-red free DMEM (Invitrogen) supplemented with penicillin–streptomycin (Life Technologies) was used for all screening experiments. Microplates were then set on flat benches for a minimum of 30 minutes at room temperature to facilitate uniform seeding in the surfaces of each microplate well, thus reducing possible edge effects, as described previously (39). The subsequent individual steps in the screening studies are described in Supplementary Materials and Methods.

Secondary GFP-based DSB repair assays

We used a collection of GFP-based assays to measure SSA, total NHEJ, and MMEJ repair, created by Bennardo and colleagues (35, 36), which have been described previously. In these experiments, each cell line was Amaxa nucleofected with the ddSceGR plasmid in standard cuvettes provided by the manufacturer (Lonza Group, Ltd.). Cells were then diluted in culture media consisting of DMEM with 10% regular FBS, and then seeded at a density of 20,000 cells per well in 96-well microplates. Cell counting was performed before nucleofection, and as such a 25% cell loss factor was incorporating into the cell dilution calculations to account for loss of cells during the nucleofection process and the transfer from cuvettes to other vessels. Cells were added in a 50-μL volume to the microplate wells containing 25 μL of culture media diluted with test compounds at the desired concentration(s) along with DSB ligands. Unless otherwise specified, these assays tested compounds at 10 μmol/L concentrations in DMSO. A single media wash was performed after 24 hours and the cells were then incubated for an additional 48 hours to allow maturation of the GFP expression. After a total incubation time of 72 hours, cells were washed with PBS (200 μL) and then dissociated using 25 μL of Accutase incubated for 15 minutes at 37°C (Innovative Cell Technologies, Inc.), followed by the addition of 25 μL of serum-free media. Accutase was used because this dissociation reagent does not require subsequent incubation with DMEM containing FBS for inactivation that can lead to higher rates of clogging in flow cytometers. In addition, the rates of reattachment to microplate wells are lower in the absence of serum, which can become an issue when handling larger numbers of plates leading to longer incubation times in the microplates during each processing step. Cells were then transferred to round bottom, polypropylene 96-well plates for analysis by flow cytometry. NHEJ and HR repair activity was assessed by quantification of the percentages of $DsRed^+$ and GFP^+ cells, respectively, using an Accuri C6 flow cytometer equipped with a HyperCyt autosampler (Intellicyt Corporation). The Hypercyt is an instrument that facilitates the automated analysis of microplates by flow cytometry, and has been described previously (40). The HyperCyt sampling settings were as followed: 35 rpm peristaltic pump speed, 15-second sip time (sampling ~3.4 μL/s), 2.5-second rinse time, and a 15-second plate shake during each rinse. Each plate was thus analyzed in approximately 45 minutes using these settings, and the entire volume of each microplate well was sampled. Cell numbers were also acquired in each well using the HyperCyt. Standard compensation techniques were used when GFP and RFP were analyzed simultaneously to minimize spectral overlap. The data were analyzed using FlowJo (TreeStar, Inc.). Experiments were performed in either triplicate or quadruplicate, and error bars represent standard errors of the mean (SEM).

IR foci formation assays

Cells were seeded into eight-chamber tissue culture slides (Fisher) and incubated overnight, and selected slides were then treated with IR using a Cesium Irradiator to deliver a dose of 10 Gy. Unless otherwise specified, these assays tested compounds with IR at 10 μmol/L concentrations in DMSO, and the final DMSO v/v amount was 0.1% in cell culture. The compounds were added 1 hour before irradiation and kept in the culture media until processing (i.e., 5 hours after IR). Cells were fixed in 4% paraformaldehyde (PFA) at room temperature for 15 minutes, followed by a block and permeabilization step with 10% bovine growth serum (BGS) and 0.5% Triton-X for 1 hour. Commercially available antibodies were used to detect the following protein targets: phospho-specific γH2AX (S139; #32827; Upstate), 53BP1 (rabbit polyclonal; NB100-904SS; Novus Biologicals), phospho-specific DNA-PKcs (T2609 and S2056; #ab18356 and #ab18192, respectively; Abcam), BRCA1 (D9; Santa Cruz Biotechnology), and phospho-specific Chk2 (T68; #2661; Cell Signaling Technology). The secondary antibodies used were Alexa Fluor 594–labeled goat anti-mouse IgG (Molecular Probes) and Alexa Fluor 488–labeled chicken anti-rabbit IgG (Molecular Probes), each at a 1:500 dilution. Cell nuclei were stained with 4′,6-diamidino-2-phenylindole (DAPI) that was included in the Vectashield mounting medium (Vector Laboratories). Images were obtained using a Carl Zeiss confocal laser scanning microscope (Carl Zeiss Microscopy, LLC) and processed using ImageJ and Adobe Photoshop software. For foci quantification, >100 nuclei were counted, with cells forming >5 foci were scored as positive. Experiments were performed in either triplicate or quadruplicate, and error bars represent SEM.

Clonogenic survival assays

U2OS and T98G cells were incubated with test compounds for 1 hour before irradiation on a cesium irradiator at multiple doses, and the cells were then trypsinized after a 4-hour incubation post-

Published OnlineFirst December 15, 2014; DOI: 10.1158/1535-7163.MCT-14-0765

IR with the compounds (10 μmol/L concentrations in DMSO; and the final DMSO v/v amount was 0.1% in cell culture.). Cells were then seeded at 500, 200, 100, and 50 cells per well and grown for 14 days. Colonies (>50 cells) were visualized by fixing with methanol and staining with crystal violet. Surviving fractions were then calculated by normalizing to the plating efficiency for each experiment (colony formation after 0 Gy dose), and as described previously (41).

Results

Development of a cell-based, high-throughput small molecule screening platform to identify novel DSB repair inhibitors

We first sought to miniaturize our dual NHEJ and HR reporter assay into a microplate format suitable for high-throughput small molecule screening. Schematics of the mNHEJ and HR repair assays, along with the inducible I-SceI system, are shown in Fig. 1A, and also have been described previously (27). Briefly, the EJ-RFP repair assay is based on a tetracycline-dependent regulatory system, and it consists of a repair substrate and a reporter vector. The I-SceI recognition site [TAGGGATAA^CAGGGTAAT] was inserted in-frame between the start codon and the open reading frame (ORF) of the tet repressor (TetR) gene in the repair substrate. The reporter vector contains an RFP gene driven by a cytomegalovirus (CMV) promoter with an intervening TetR-binding site. When the repair substrate and reporter vector are chromosomally integrated, RFP expression is basally repressed by the TetR protein under normal conditions. Cleavage of the I-*Sce*I site and subsequent rejoining of the free DNA ends by error-prone NHEJ results in disruption of the TetR ORF and consequent expression of RFP. In the DR-GFP system, the 24-bp recognition site of I-SceI has been integrated into the GFP gene such that it disrupts the gene. Repair of the cleaved I-*Sce*I site by HR gives rise to a functional GFP gene, when the template used for repair is a truncated GFP fragment located downstream in the plasmid (33). RFP- and GFP-positive cells are typically measured by flow cytometry to assess mNHEJ and HR repair activity, respectively. Our inducible I-SceI protein contains a modified destabilizing FKBP12 domain on the N-terminus, and the ligand-binding domain of the glucocorticoid receptor (GR) on the C-terminus (referred to as ddSceGR; ref. 42). The addition of the small molecule, Shield1, blocks the destabilizing effect of the N-terminal domain, and the addition of the synthetic glucocorticoid receptor ligand, triamcinolone acetonide, induces translocation from the cytoplasm to the nucleus. We recently created a U2OS cell line containing single copies each of EJ-RFP, DR-GFP, and ddSceGR (referred to as U2OS EJ-DRs cells), and we extensively validated its function as a reliable and dynamic reporter of DSB repair, using a panel of small interfering RNAs (siRNA) and selected small molecule DSB repair inhibitors (27).

We previously characterized the timing and kinetics of our DSB repair assay, with regard to DNA cleavage activity and maturation of the RFP and GFP signal (27), which is depicted in Fig 1B for reference. A longer incubation time is required for the maturation of EJ-RFP expression (96 hours), owing to the requirement for wild-type (WT) TetR protein to be degraded before derepression of the RFP gene in the reporter vector can occur (i.e., following disruption of the TetR ORF by mNHEJ repair events). In our previous studies involving U2OS EJ-DRs cells, we analyzed the percentages of RFP- and GFP-positive cells by flow cytometry (27). Although this approach is associated with high levels of sensitivity and low error rates, it is not well suited for the analysis of small numbers of cells grown in 384-well microplates. We thus developed a protocol to image RFP- and GFP-positive cells in microplates using an automated laser scanning cytometer. We reasoned that this approach would be advantageous for the analysis of large numbers of samples, because adherent cells can be measured rapidly without the need for trypsinization and subsequent transfer to flow cytometry tubes for analysis. Furthermore, most laser scanning cytometers can process large numbers of microplates automatically with the addition of a robotic plate exchanger. We also considered using a conventional fluorescence plate reader to measure the total amount of RFP and GFP fluorescence in each microplate well, which has been described previously in high-throughput screens with multicolor competition assays (43). However, our initial tests using this approach indicated that while RFP fluorescence could be measured successfully, GFP fluorescence was not reliably detected in U2OS EJ-DRs cells (data not shown). This likely can be explained by the finding that the DR-GFP assay reports %GFP-positive cells in the range of 1% to 10%, which is below the threshold to achieve a reasonable signal-to-noise ratio for most conventional microplate readers. In contrast, laser scanning cytometers typically image the entire well and can identify any fluorescent objects in the field, which significantly raises the sensitivity of detecting smaller subpopulations of fluorescent protein-expressing cells (e.g., in the range of 1%–10%).

To this end, we used the ImageXpress Velos laser scanning cytometer for our studies (Molecular Devices). The Velos can image a single 384-well plate in approximately 5 to 10 minutes, capturing fluorescence in two separate channels (e.g., RFP and GFP), and it is equipped with "on-the-fly" image analysis. We validated and optimized image segmentation and spot recognition algorithms with the Velos software analysis tools to detect RFP- and GFP-positive cells, using various controlled mixes of RFP- and GFP-positive U2OS EJ-DRs cells, which were isolated by fluorescence-activated cell sorting (FACS) after DSB ligand treatment. It should be noted that RFP in the EJ-RFP assay was derived from DsRed and is expressed in the entire cell (27), while GFP expression in the DR-GFP assay is restricted to the nucleus because of a nuclear localization signal added to the N-terminus (33). These differences made it important to optimize the image segmentation algorithms for each fluorescent protein, with cells grown at a controlled range of densities in 384-well microplates. For example, higher cell densities would confound the ability to segment RFP-positive cells in close contact because of pan-cellular fluorescent protein expression, while this issue would be less problematic for nuclear-localized GFP-expressing cells. A representative whole well image of RFP- and GFP-positive EJ-DRs cells acquired by the Velos is shown in Fig. 1C, and the inset shows the segmentation process we developed for GFP-positive cells. Sample whole well images of various mixes of fluorescent protein-positive and -negative cells are shown in Supplementary Fig. S1A, which illustrates the high sensitivity in detecting very low frequencies of GFP-positive cells. We tested a range of cellular fixation conditions in our initial studies, as fixation would permit the analysis of microplates at later times without significant loss of RFP and/or GFP fluorescence. We found that fixation with 4% PFA for 5 to 10 minutes followed by a single wash with PBS was sufficient to preserve RFP and GFP fluorescence. Interestingly, fixation times beyond 10 minutes and/or omission of the PBS wash led to significant reductions in RFP fluorescence at later time

Published OnlineFirst December 15, 2014; DOI: 10.1158/1535-7163.MCT-14-0765

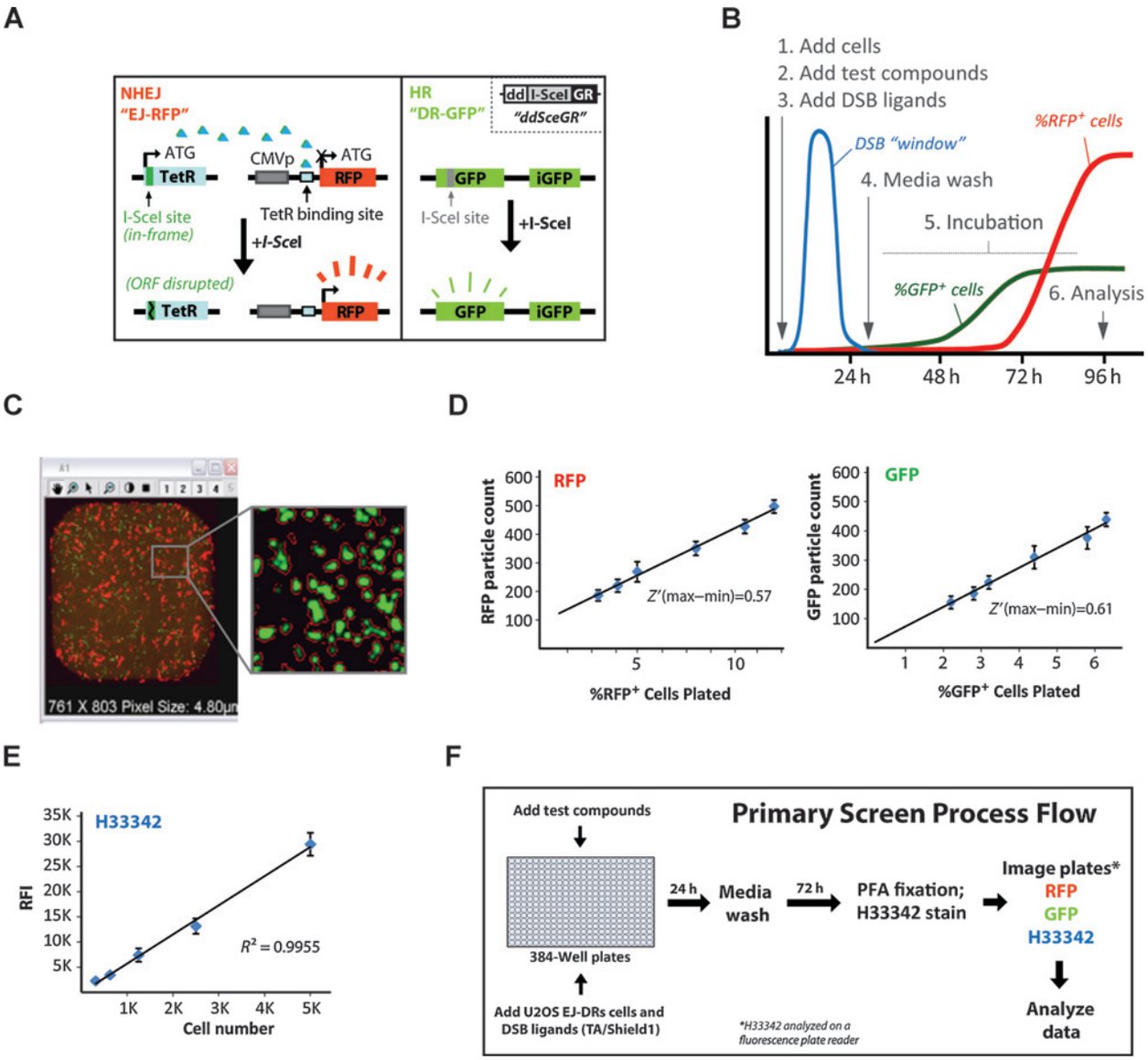

Figure 1.
Initial design and miniaturization of a cell-based assay for DSB repair inhibitor screening. A, schematic of the EJ-RFP (left) and DR-GFP (right) assays to measure mNHEJ and HR, respectively. Inset on the right, the ddSceGR system for ligand-dependent DSB induction. B, schematic depicting the timeline associated with the use of the EJ-DRs assay to evaluate the effect of small molecules on DSB repair activity, which consists of six steps: (i) cell seeding, (ii) test compound addition, (iii) DSB induction, (iv) ligand and compound wash-out, (v) incubation to permit repair and reporter gene expression, and (vi) analysis of RFP- and GFP-positive cells indicating DSB repair events. C, sample image for a single well of a 384-well plate, acquired by the ImageXpress Velos, with the GFP- and RFP-channels overlaid; inset/zoom-in, example of segmentation algorithm to enumerate GFP-positive cells. D, linearity of detection and enumeration of RFP- and GFP-positive cell in 384-well plates (left and right, respectively), as detected with the ImageXpress Velos. The percentages of RFP- and GFP-positive cells for each data point are shown on the *X*-axis, which were derived from cells analyzed by flow cytometry in parallel. Z′-factors are shown in each plot between the maximum and minimum data points to highlight the sensitivity and reliability of the assay and detection platform for drug screening. E, linearity and correlation of plated cell numbers with H33342 fluorescence, as detected using a fluorescence plate reader. F, overview of the process-flow for our high-throughput screen.

points, which could not be abrogated with quenchers such as glycine (data not shown).

We also sought to incorporate a method for cell normalization to control for differences in cell number between wells, which could arise from either drug toxicity or intra- and/or inter-micro-plate variations in liquid handling. We were limited to the use of fluorescent proteins or fluorophores that did not have significant spectral overlap with RFP or GFP, which would confound our analyses of DSB repair. We selected the nuclear ultraviolet dye, Hoechst 33342 (H33342), which does not interfere with the detection of GFP or RFP fluorescence. We designed a protocol in which H33342 was added at the time of PFA fixation (i.e., after the PBS wash step). As noted earlier, the Velos can image with only two channels, and thus we chose to measure H33342 fluorescence with a conventional fluorescence plate reader after analysis on the Velos. As shown in Fig. 1D, we confirmed that our optimized

Published OnlineFirst December 15, 2014; DOI: 10.1158/1535-7163.MCT-14-0765

imaging, fixation, and analysis protocols could detect a wide range of %RFP- and %GFP-positive U2OS EJ-DRs cells (left and right, respectively). We specifically tested RFP and GFP mixes corresponding to maximal versus minimal mNHEJ and HR repair activity that would be associated with the EJ-DRs reporter assay under normal assay conditions. These "high" and "low" values correspond to cells treated with or without DSB ligands, respectively (without any test compounds); and essentially these conditions served as our initial negative and positive controls for the first assay optimization studies. Background levels of RFP- and GFP-positive cells are found in U2OS EJ-DRs cells, which are associated with low levels of DNA cleavage by ddSceGR in the absence of ligands (27). In this manner, maximal inhibition of mNHEJ/HR repair would reduce RFP/GFP percentages to that observed in cells that were not treated with the DSB ligands. The *Z′*-factor, a common measure of assay reproducibility (44), was >0.5 between the high and low values for both RFP- and GFP-positive cell mixing experiments, which indicated suitability for high-throughput screening. We also detected a highly linear correlation between plated cell number and H33342 fluorescence in these experiments (Fig. 1E). Taken together, these data suggested that our miniaturized EJ-DRs assay and analysis protocols would be suitable for high-throughput screening in 384-well microplates.

On the basis of our initial optimization experiments described above, we envisioned a screening process flow in which cells are seeded directly into 384-well microplates with test compounds of interest, along with ligands to induce DSBs. After a period of induced DNA cleavage in the presence of compounds (24 hours), a media wash is performed to terminate DSB activity. This wash step also removes the compounds, which would minimize the possibility of toxicity and fluorescence artifacts associated with some compounds in long-term culture. Cells are then incubated for a period of time to allow expression of RFP and GFP, followed by PFA fixation, H33342 staining, and finally fluorescence measurements to assess DSB repair activity and cell numbers. In this manner, the effects of small molecules on both mNHEJ and HR activity can be assessed simultaneously, and cell viability can be used to exclude toxic compounds from any identified hits. This process flow is summarized in Fig. 1F. As discussed below, we next validated this process flow using known chemical inhibitors of DSB repair, and also in a pilot small molecule screen.

Validation of our miniaturized DSB repair screening assay using known inhibitors of NHEJ and HR repair

We next sought to confirm we could detect the expected effects of known chemical inhibitors on DSB repair activity in 384-well microplates, using our screening process flow. To this end, we tested mirin, a recently described inhibitor of the Mre11–Rad50–Nbs1 (MRN) complex (45). We tested mirin along with DMSO controls in 384-well plates, at a range of doses in triplicate. The percentages of RFP- and GFP-positive cells from triplicate samples in wells containing various doses of mirin were normalized to the percentages observed in wells containing DMSO-treated cells for both mNHEJ and HR, respectively. In this manner, the data can be presented as a relative assessment of DSB repair on a two-dimensional (2D) plot (which we have referred to as a RADaR plot, based on our previous work; ref. 27), which allows one to rapidly assess the effects of a given condition on both mNHEJ and HR repair activity visually. A schematic of how EJ-DR measurements in each quadrant are categorized is shown in Fig. 2A for reference. Before testing with mirin, we first performed a DMSO tolerance test to assess the possible contribution of artifacts in DSB repair activity arising from DMSO toxicity. These experiments confirmed that DMSO concentrations as high as 2% did not significantly affect cell viability and/or DSB repair activity (Supplementary Figs. S1B and S1C, respectively). In contrast, DMSO concentrations of 3% or more led to substantial reductions in cell numbers, which corresponded to reductions in both mNHEJ and HR repair activity. As shown in Fig. 2B, mirin inhibited both mNHEJ and HR repair activity in a dose-dependent fashion from 25 to 100 μmol/L. These data were normalized to H33342 staining results, which revealed approximately 50% and 70% reductions in cell viability at 50 and 75 μmol/L doses of mirin, respectively. Mirin is known to be toxic to cells at doses above 25 μmol/L (45), which can confound the ability to differentiate a direct effect on DSB repair activity versus indirect suppression via disruption of normal proliferation, as highlighted in the DMSO tolerance test above. After normalizing for cell toxicity, the data revealed that mirin preferentially inhibits HR over mNHEJ repair activity, with a half maximal inhibitory concentration (IC_{50}) for HR repair inhibition of approximately 50 μmol/L, which is consistent with previous studies using the DR-GFP reporter assay (45). The H33342-normalized IC_{50} curves for mNHEJ and HR repair activity after mirin treatment are shown in Supplementary Fig. S1D. These data highlight the suitability of our miniaturized assay to detect small molecule–induced changes in DSB repair activity. They also highlight the importance of assessing cell toxicity as a potential confounder for changes in DSB repair activity.

Execution of a pilot screen using a library of known bioactive compounds

We next sought to assess the performance of our 384-well plate EJ-DRs assay in a pilot compound screen, in preparation for scaling up to interrogate 20,000 compound library. Initial studies with several 384-well microplates containing U2OS EJ-DRs cells treated with and without the DSB ligands indicated excellent signal-to-noise ratios and high levels of assay stability (Fig. 2C). Minor edge effects were noted in selected plates, which were attributed to the prolonged culture time (96 hours) required for maximal RFP expression in the EJ-RFP portion of the DSB repair assay (Fig. 2C and Supplementary Fig. S1E). This issue was addressed by incorporating breathable plate seals, which minimized the evaporation of media in the corners of the 384-well plates during these prolonged cell culture periods. Next, we performed a pilot drug screen with a commercially available library containing approximately 1,200 compounds (Library of Pharmacologically Active Compounds, LOPAC 1280; Sigma-Aldrich). U2OS EJ-DRs cells were added to microplates containing compounds at a 10 μm concentration, and the last two columns of each microplate were reserved for positive and negative controls. The positive control consisted of U2OS EJ-DRs cells treated without DSB ligands, while the negative control consisted of cells treated with DSB ligands and 1% DMSO. In the former case, excluding the DSB ligands would simulate maximal inhibition of NHEJ and HR repair in this assay. In the latter case, the addition of DMSO along with the DSB ligands (and without any DSB repair inhibitors) would represent basal NHEJ and HR repair activity under normal conditions. We used the optimized screening protocol described above, and library screening was performed in duplicate over 2 days to test assay reproducibility. The *Z′*-factors

Published OnlineFirst December 15, 2014; DOI: 10.1158/1535-7163.MCT-14-0765

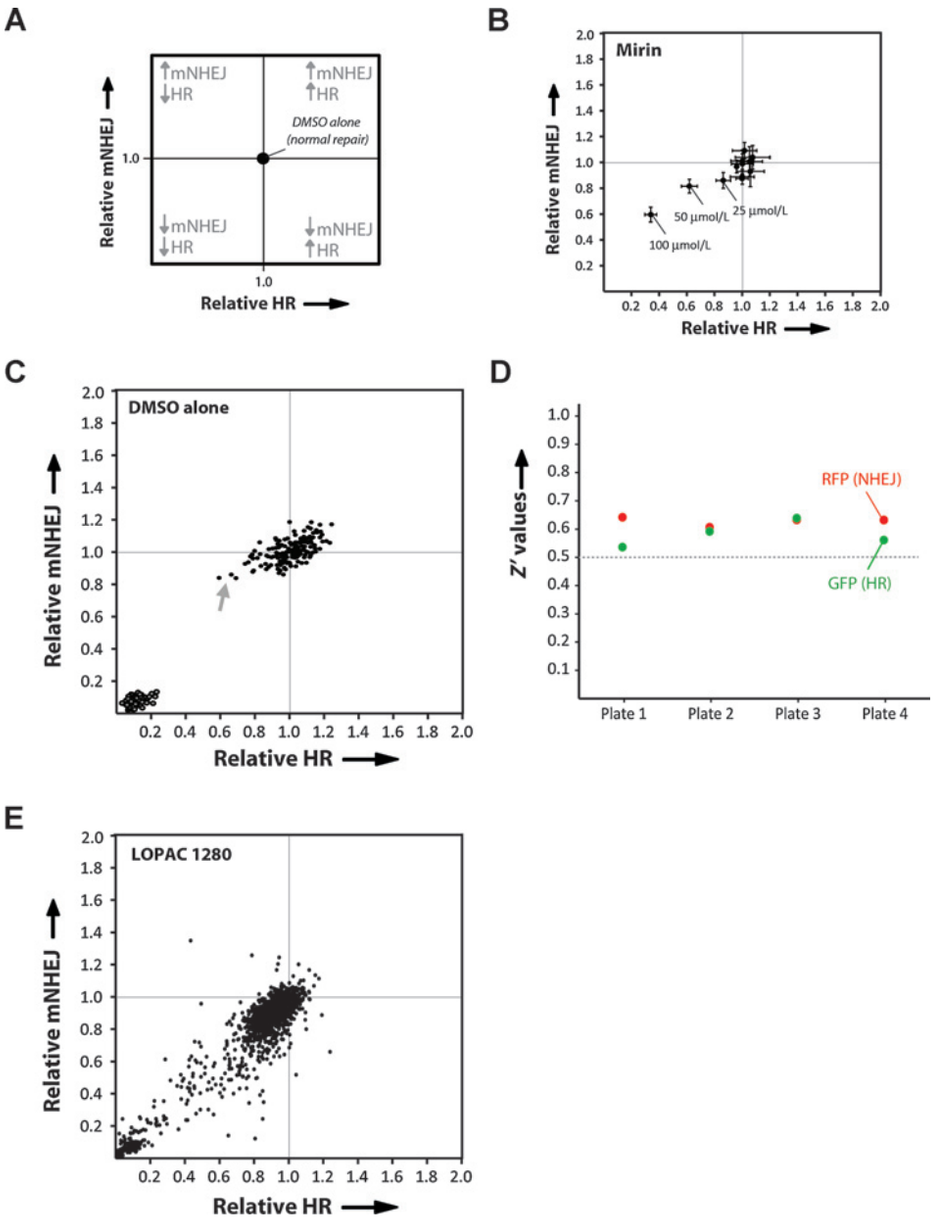

Figure 2.
Validation of a high-throughput screening strategy with control DSB repair inhibitors and a completion of a pilot small molecule screen. A, schematic of our Relative Assessment of DNA Repair (RADaR) plot to assign hits to different categories each with unique DSB repair modulation phenotypes. B, effects of various concentrations of mirin on mNHEJ and HR repair, as visualized on the RADaR plot presented in A. C, performance and stability of our miniaturized EJ-DRs assay in 384-well plates. Data from wells treated with DMSO alone, with or without DSB ligands are shown. Gray arrow indicates wells in corners of 384-well plates suggestive of a possible edge-effect. D, Z′-factors calculated from the positive and negative controls for one set of replicates from the pilot LOPAC screen. Dashed line highlights a Z′-factor of >0.5 that indicates suitability for high-throughput screening. E, results of our pilot LOPAC screen, presented as a 2D RADaR plot; see hit categories in A.

were greater than 0.5 between the positive and negative control wells for each assay plate for both duplicates (Fig. 2D and data not shown), indicating excellent assay stability and reproducibility. A cutoff of greater than a 50% change in mNHEJ and/or HR repair activity was set as the threshold for hits, based on our initial optimization experiments with control drugs and our previous work (27). As shown in the RADaR plot in Fig. 2E, several compounds were identified that substantially altered the normal pattern of DSB repair compared with DMSO-treated cells. These results were highly reproducible across the duplicate experiments (data not shown), and the hit rate was approximately 2%. The most active hits are shown in Table 1, which are notable for currently and previously FDA-approved drugs (e.g., pimozide and mibefradil, respectively). Unexpectedly, we found that etoposide substantially inhibited HR repair activity, which was validated further in secondary assays (discussed below). Several of these drugs were validated and evaluated further in combination with the hits identified from the main compound screen presented below.

Table 1. List of top hits from the LOPAC screen, which significantly affected mNHEJ and/or HR repair activity

LOPAC 1280—top hits		
	Repair activity	
Drug name	**NHEJ**	**HR**
Pimozide	0.28	0.55
Loperamide	0.20	0.57
Mibefradil	0.28	0.57
Etoposide	0.65	0.08
SR 59230A	0.27	0.58
AMN082	0.19	0.92

Published OnlineFirst December 15, 2014; DOI: 10.1158/1535-7163.MCT-14-0765

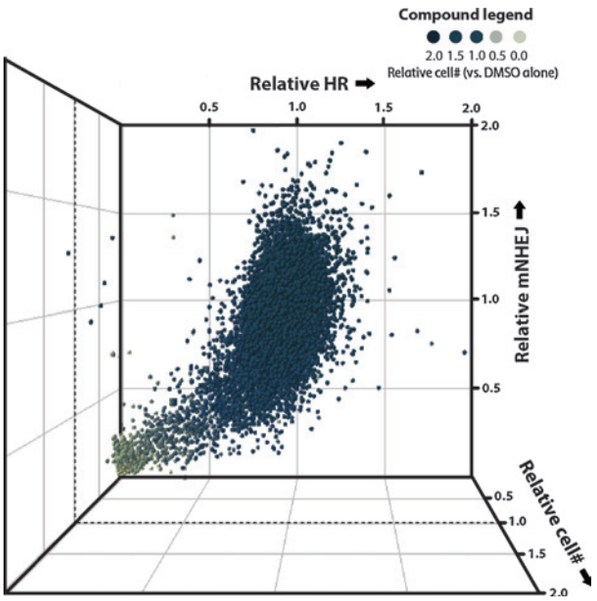

Figure 3.
Results of a high-throughput screen of approximately 20,000 small molecules for novel DSB repair inhibitors. Results of an approximately 20,000 compound screen for novel DSB repair inhibitors, presented here as a 3D Relative Assessment of DNA Repair (RADaR) plot; all results have been normalized to U2OS EJ-DRs cells treated with DMSO alone (and DSB ligands). The *Y*-axis shows relative mNHEJ repair activity, the *X*-axis shows relative HR repair activity, and H33342 fluorescence is plotted on the *Z*-axis for relative cell number. Each dot represents a single test compound, which has also been color coded according to relative cell number, as depicted in the compound legend.

Interrogation of a diverse small molecule library for novel DSB repair inhibitors

After demonstrating feasibility in the pilot LOPAC drug screen, we performed a high-throughput small molecule screen using our miniaturized EJ-DRs assay. We interrogated a library containing approximately a subset of 20,000 diverse compounds, from a 150,000 member library from the Rockefeller University HTSRC. On the basis of our initial results in the pilot LOPAC screen, each compound was tested in singlicate at a 10-μm concentration. We again used the optimized screening protocols described above. The entire library, with positive and negative controls, consisted of 55 384-well plates. The Z′-factor for individual plates was monitored throughout the screen to assess for potential assay drift and other possible confounders, and was >0.5 as in the pilot LOPAC screen (data not shown). Hit thresholds similar to those used in the pilot LOPAC screen were applied to identify novel DSB repair modulators, and hits that decreased viability by greater than 50% were excluded from the hit-list. The results of the screen are shown in Fig. 3 as a three-dimensional (3D) plot with HR (GFP), mNHEJ (RFP), and cell number (H33342) plotted on the *X*-, *Y*-, and *Z*-axes, respectively. A 2D plot depicting HR versus mNHEJ alone is also shown in Supplementary Fig. S2 for reference. Approximately 750 hits were identified that significantly altered DSB repair, corresponding to a hit rate approximately 3.8%. Hit rates from cell-based assays typically range between 1% and 2% for a single phenotype, although the number of hits from a given screen is highly dependent on multiple variables, including the screening phenotype itself, the type of cell-based measurement, and the hit thresholds that are set (46). In our screen, we envisioned four possible types of hits: (i) selective HR inhibitors, (ii) stimulators of HR and/or mNHEJ (e.g., which could occur via disruption of cNHEJ as described previously; refs. 27, 47), (iii) selective inhibitors of mNHEJ, and (iv) dual inhibitors of both HR and mNHEJ (see schematic in Fig. 2A). Thus, we expected a higher hit-rate than would be observed for a typical cell-based screen with a single readout and phenotype.

Our hit confirmation and validation strategy is summarized in Fig. 4. We first cherry-picked and re-tested each of the 750 hits at three concentrations (1, 5, and 10 μm) in duplicate as a means to rule out random false-positives. This also allowed an initial ranking of potency. These experiments led to the identification of 100 confirmed hits with descending concentration-responses and high rates of reproducibility between replicates. We then tested these confirmed hits at a larger range of concentrations in triplicate, to rank those compounds demonstrating a statistically significant full sigmoidal concentration-response. For these experiments, we used the same 384-well plate-based protocol from the primary screen to assess mNHEJ and HR activity. We then selected compounds with reproducible IC_{50}s less than 20 μm. We also excluded hits corresponding to pan assay interference compounds (PAINS) from a database created by the Rockefeller University HTSRC. These compounds, often referred to as "frequent hitters," are known to nonspecifically block activity in many high-throughput screening studies (48). These experiments led to the identification of 63 refined hits. We then ordered powder stocks for each of these hits, solubilized them in DMSO, and performed concentration-response studies once again to confirm reproducibility with the freshly prepared compound stocks. At this stage, we measured mNHEJ and HR repair in the EJ-DRs assay using flow cytometry in 96-well plates. This approach facilitated the assessment of possible fluorescence artifacts and confounding cell viability effects, because detailed cell-level fluorescence could be quantitatively analyzed in the entire population of cells for each treated well. We used an automated 96-well plate flow cytometer for these studies, which is discussed further in the section below. Cell numbers were also enumerated for each compound to further assess compound toxicity. Furthermore, a larger number of cells could be analyzed for RFP and GFP fluorescence for each sample (e.g., 10–20K cells per tube), which increases the sensitivity of the analysis. In parallel, we performed structure clustering analyses to assess whether hits with similar structures displayed similar EJ-DRs repair assay phenotypes.

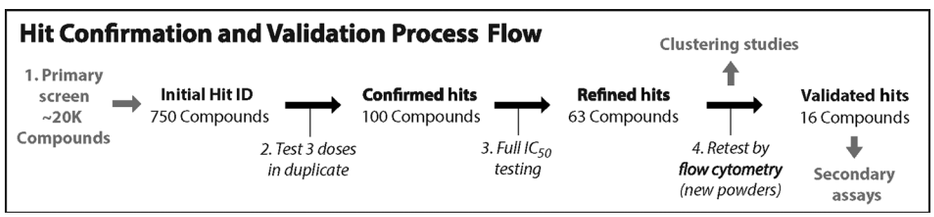

Figure 4.
Overview of hit confirmation and validation process. Flow chart schematic overview of our hit confirmation and validation strategy.

Published OnlineFirst December 15, 2014; DOI: 10.1158/1535-7163.MCT-14-0765

Table 2. List of confirmed and validated hits that inhibit key DSB repair pathways

List of validated hits									
			IC_{50}					IC_{50}	
#	Drug ID (RU#)	Common name	mNHEJ	HR	#	Drug ID (RU#)	Common name	mNHEJ	HR
1	RU-0000476	Pimozide	21.3	16.5	9	RU-0001843	Benzamil hydrochloride	23.7	19.6
2	RU-0093452	Unknown	6.0	46.4	10	RU-0084642	SR 59230A Oxalate	7.4	52.8
3	RU-0093845	Unknown	6.6	9.5	11	RU-0000824	Loperamide hydrochloride	2.8	n.r.
4	RU-0097818	Unknown	0.6	6.3	12	RU-0084490	AMN082	6.6	31.3
5	RU-0104496	Unknown	18.3	21.8	13	RU-0094349	Unknown	6.3	58.3
6	RU-0000092	Cyproterone acetate	10.8	13.1	14	RU-0154704	Unknown	14.9	41.7
7	RU-0001125	3α-Acetoxydihydro-deoxygedunin	6.5	4.3	15	RU-0084411	Mibefradil dihydrochloride	4.1	n.r.
8	RU-0102758	Unknown	1.4	1.2	16	RU-0005520	Unknown	10.5	n.r.

NOTE: Summary of the 16 hits that we confirmed and validated using the strategy described in Fig. 4. Rockefeller IDs are shown for each compound that can be cross-referenced with the corresponding SMILES strings in Supplementary Fig. S8. Common names for each compound are shown when one exists, and the IC_{50}s for mNHEJ and HR repair activity are shown. The structures for each compound are shown in Supplementary Fig. S3.
Abbreviation: n.r., not reached.

Compounds that clustered in this manner were prioritized, because these data provided another layer of supporting evidence for phenotypic specificity, as described previously (49).

The experiments described above led to the identification of 16 validated hits, which we then tested below in orthogonal secondary assays. The structures for each of these 16 hits are shown in Table 2, along with the IC_{50} results for mNHEJ and HR repair. The full IC_{50} curves for each of these hits for mNHEJ, HR repair, and cell number, as measured by flow cytometry, are shown in Supplementary Fig. S3. The analysis of mibefradil using our hit confirmation and validation strategy, starting from its identification in the primary screen as a selective mNHEJ repair inhibitor to its validation by flow cytometry, is shown in Fig. 5A. The IC_{50} curves for each of the 100 confirmed hits are shown in Supplementary Fig. S8, which also contains the SMILES IDs for reference. One example of a structure cluster with similar effects on mNHEJ/HR repair and cell viability is shown in Fig. 5B. The index compound in this cluster, RU-0154704, is notable for highly selective repression of mNHEJ repair, with minimal effects on HR or cell viability. The major structure clusters that we identified with similar EJ-DRs phenotypes are shown in Supplementary Fig. S8B, and all identified clusters are shown in Supplementary Fig. S8C for reference. Our hit-list was notable for several known drugs that inhibited DSB repair, including pimozide, mibefradil, loperamide, AMN082, and cyproterone (several of these drugs were detected in the pilot LOPAC screen; see Table 1). In addition, many of the identified hits selectively inhibited mNHEJ and/or HR without any discernable effects on cell viability, except at high doses. For example, compound RU-0093845 (listed as #3 in Table 2) significantly inhibited both mNHEJ and HR repair to levels similar to cells treated without DSB ligands, with minimal effects on cell viability even at a 50 μmol/L dose. As a final assessment to rule out false-positive hits that suppress RFP and/or GFP fluorescence, we tested the hits in a counter-screen in which U2OS EJ-DRs cells were treated with ligands for 24 hours to induce DSBs, in the absence of test compounds, followed by incubation with the test compounds. RFP and GFP fluorescence was then measured as performed in the primary screen (process flow shown in Supplementary Fig. S4A). None of our hits affected RFP or GFP fluorescence, and several examples are shown in Supplementary Fig. S4B. Next, we tested each of these 16 hits in a comprehensive panel of orthogonal secondary assays to further assess their functional effects on DSB repair activity.

Evaluation of identified hits in orthogonal secondary assays

Next, we sought to test the activity of our 16 validated hits in secondary DSB repair assays. Our secondary assay process flow is outlined in Fig. 6A. We chose to test them first in a panel of unique, GFP-based DNA repair assays that again use I-SceI to induce a site-specific DSB. The goal of these studies was to demonstrate functional activity as an additional validation step, and also possibly to further elucidate the mechanism(s) by which these compounds regulate DSB repair. As discussed earlier, our EJ-RFP assay detects any mNHEJ events in a robust manner, which makes it particularly useful as an initial screen for novel DSB repair inhibitors. However, it does not necessarily discriminate specifically between the NHEJ repair subpathways. Bennardo and colleagues (35) recently created a series of elegantly designed DSB repair assays that specifically measure total NHEJ, MMEJ, and SSA in U2OS cells. The total NHEJ repair assay contains a promoter separated from a GFP gene by an intervening puromycin (puro) gene. The puro gene is flanked by two I-*Sce*I sites in the same orientation, such that cleavage of both sites by I-SceI results in a two-ended, cohesive DSB. Any NHEJ repair events that join the two DSB ends bring the promoter in close proximity to the GFP gene resulting in expression (with loss of the puro gene). The MMEJ reporter consists of a single GFP gene disrupted by an I-*Sce*I site with stop codons in all three reading frames, and also with a flanking 8-bp sequence that serves as a microhomology substrate. NHEJ events after DSB induction with I-SceI that use this specific microhomology sequence restore the GFP ORF. As mentioned in the Introduction, MMEJ may represent a subpathway of mNHEJ in which flanking sequence microhomology is extensively used; and thus it is possible that this MMEJ reporter could reveal changes in repair that are not necessarily reflected in our mNHEJ reporter (and *vice versa*), which measures any mutagenic repair event, regardless of microhomology usage. Finally, the SSA reporter consists of a GFP gene split into two overlapping fragments and separated by approximately 2 kbp, and the downstream 3′-fragment contains an I-*Sce*I site. In this manner, SSA events that occur between the two regions of homology eliminate the I-*Sce*I site and restore the GFP gene (with deletion of the intervening sequence). Importantly, these assays have been validated previously using both RNAi and small molecule DSB repair inhibitors (35–37, 50–52).

We sought to evaluate each of our hits, along with several control drugs, in each cell line over multiple replicates for each of the reporter assays described above. Once again, we wanted to use our ligand-dependent I-SceI cleavage system to precisely control DSB activity during incubation with the compounds. To this end, we designed a medium-throughput protocol for these studies, which is outlined in Fig. 6B. Briefly, U2OS cell lines containing each of the stably integrated DSB reporters are transfected with the

Published OnlineFirst December 15, 2014; DOI: 10.1158/1535-7163.MCT-14-0765

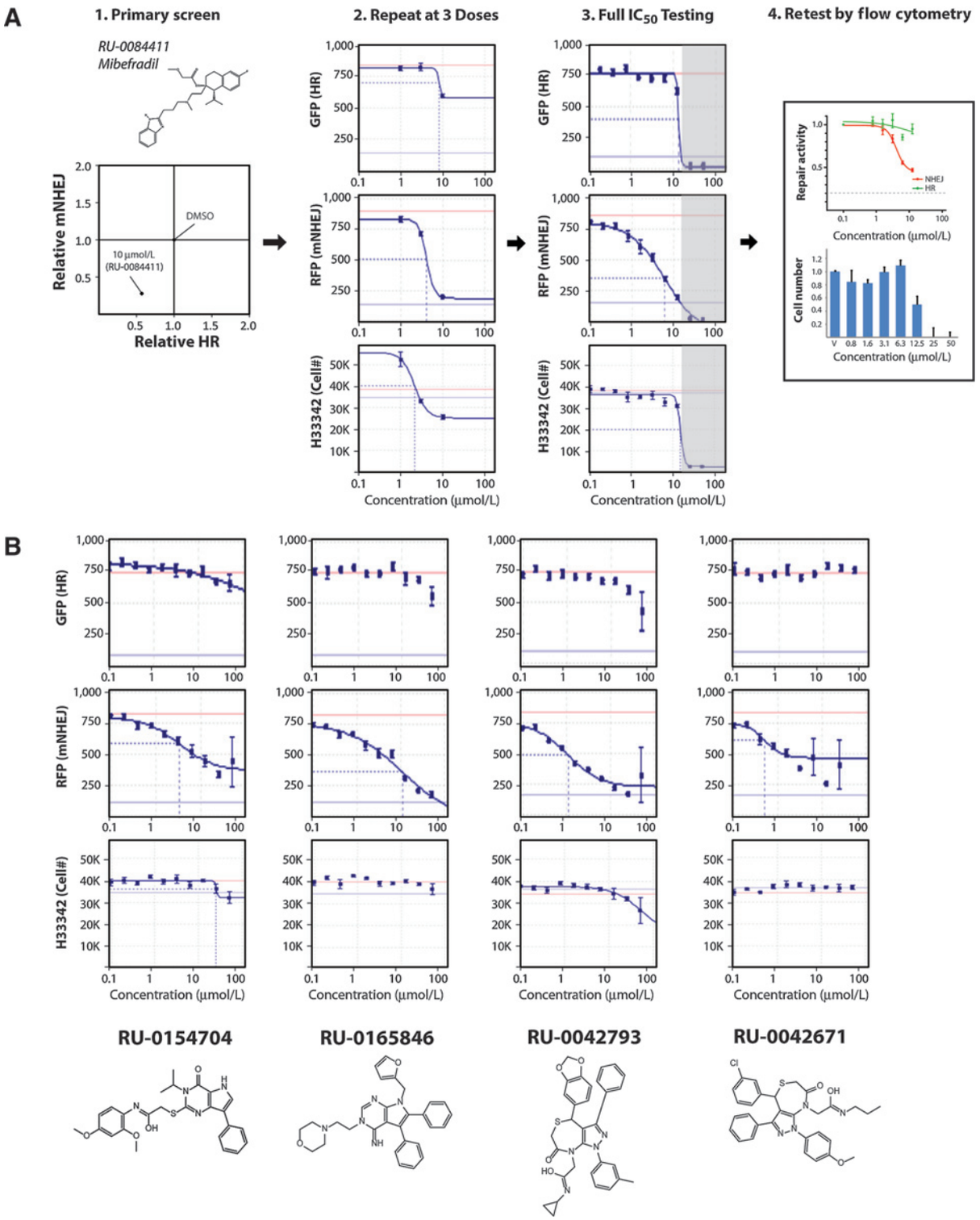

Figure 5.
Examples of the confirmation and validation process for novel DSB repair inhibitors. A, example of the confirmation and validation process for a single hit, RU-0084411 (mibefradil), numbers correspond to the strategy presented in Fig. 4. B, example of structure clustering studies in which multiple compounds share a selective effect on mNHEJ repair activity, with little repression of HR repair or cell toxicity, as detected in the full IC_{50} curves. Data are shown as acquired on the ImageXpress Velos for mNHEJ and HR repair, and a conventional plate reader for H33342 fluorescence to assess cell number. Superior and inferior horizontal lines in each plot represent the maximal and minimum signal for each assay. Rockefeller IDs are shown for each compound along with their structures, which can be cross-referenced with the corresponding SMILES strings in Supplementary Fig. S8.

Published OnlineFirst December 15, 2014; DOI: 10.1158/1535-7163.MCT-14-0765

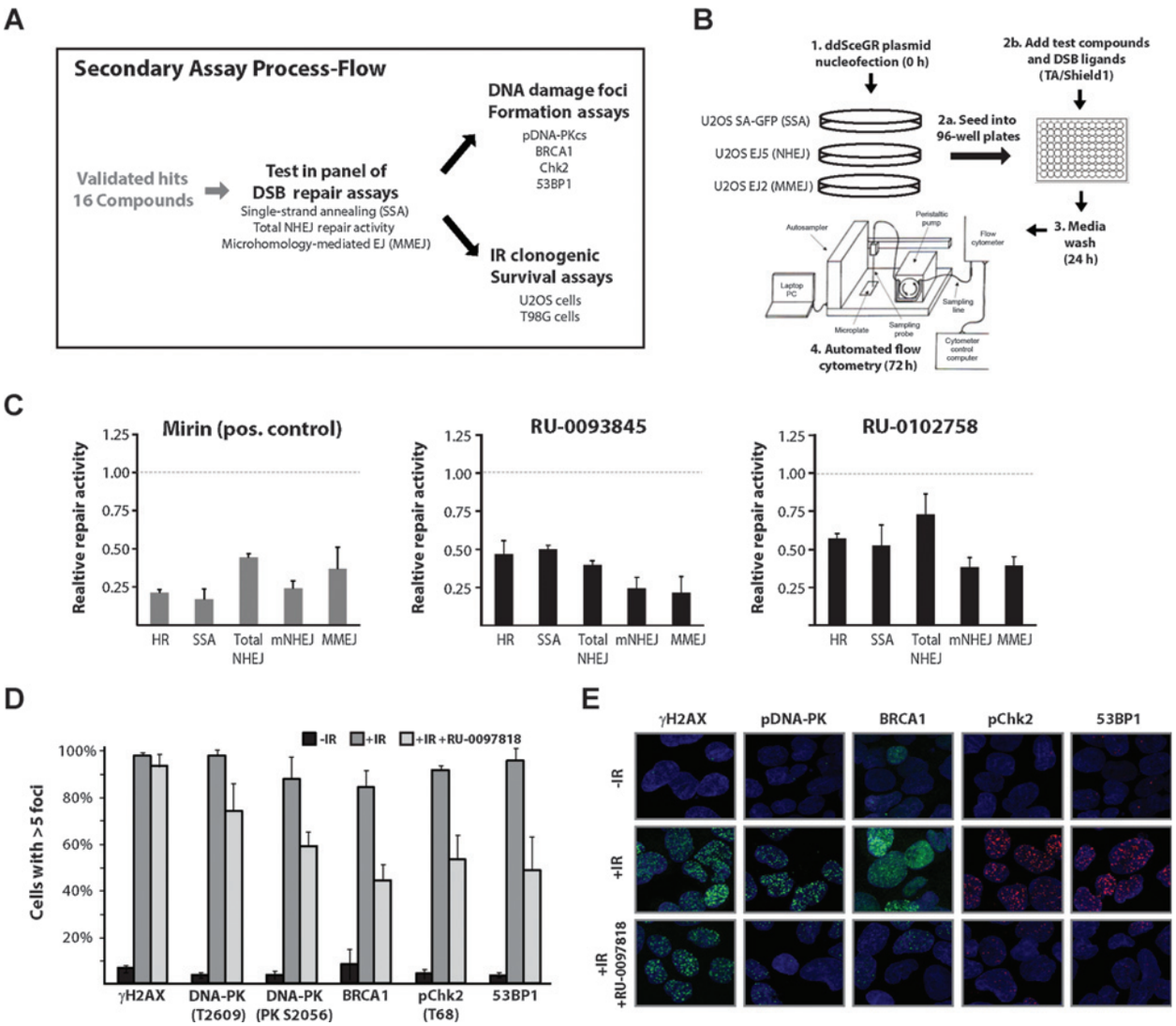

Figure 6.
Analysis of hits in secondary GFP-based DSB repair and IR foci formation assays. A, overview of the process flow to test our hits in secondary assays. B, schematic of the analysis process to interrogate the effects of each hit in a panel of GFP-based DSB repair assays. C, results for selected hits in the GFP-based repair assays to measure SSA, total NHEJ (global NHEJ, gNHEJ), and MMEJ. The results for mNHEJ and HR, as detected in the EJ-DRs assay, are also shown for comparison. Repair activities were normalized to DMSO-treated cells, as indicated by the dashed lines. Compounds were tested at 10 μmol/L concentrations. The result for one positive control, mirin, is also shown for reference (left). D, example of the results for one confirmed and validated hit (RU-0097818) in IR foci formation assays. In these assays, we tested the compound at a 10 μmol/L concentration. Antibodies specific to each of the proteins and/or posttranslational modifications are shown in each plot. The percentages of cells with >5 foci are shown. Black bars, cells treated with no IR; gray bars, cells treated with IR alone (10 Gy); and light gray bars, cells treated with IR and the test compound. E, representative confocal microscopy images from the results presented in D are shown.

ddSceGR plasmid and then seeded into 96-well plates containing test compounds along with the DSB ligands, followed by a media wash after 24 hours. The percentages of GFP-positive cells are then measured using a HyperCyt autosampler coupled to an Accuri C6 flow cytometer (see Materials and Methods for additional information about this platform). This allowed us to rapidly test our compounds in each of the key GFP-based DSB repair assays in multiple replicates, with high sensitivity and specificity. As noted earlier, we also used this platform to generate full IC_{50} curves for our 16 refined hits using flow cytometry to assess EJ-DRs repair events. We first validated the sensitivity of this approach using several known DSB repair inhibitors, including mirin (Fig. 6C), and also several DNA-PK inhibitors (Supplementary Fig. S5A). As expected, mirin substantially repressed the activity of all key DSB repair pathways, consistent with blockade of MRN complex function leading to a proximal DSB repair defect (45). Conversely, the DNA-PK inhibitors induced mNHEJ repair, and in some cases also SSA and/or HR repair, consistent with previous studies (Supplementary Fig. S5A and data not shown; refs. 27, 53, 54). Interestingly, topoisomerase inhibitors were found to preferentially suppress HR repair in the pilot LOPAC screen, and thus were included in our initial studies with these secondary assays. The results of these studies are shown in Supplementary Fig. S5B, which revealed substantial inhibition of multiple DSB repair

Published OnlineFirst December 15, 2014; DOI: 10.1158/1535-7163.MCT-14-0765

pathways (discussed further below). Collectively, these data support the utility of these secondary assays to assess the function of putative DSB repair inhibitors.

We then tested each of the validated hits from our primary screen in the GFP-based secondary assay panel using the protocols described above. The results for active hits are shown in Supplementary Fig. S6, and selected examples are presented in Fig. 6C. Each hit was tested in four independent replicates. In these assays, we tested compounds at 10 μmol/L concentrations in DMSO. Compound RU-0093845 demonstrated substantial inhibition of both mNHEJ and HR repair in the primary screen, and was notable also for suppression of SSA, total NHEJ, and MMEJ repair. As discussed earlier, this was an intriguing compound because there were virtually no effects on cell viability even at a 50 μmol/L dose. The counter-screening studies presented earlier and shown in Supplementary Fig. S4 ruled out a possible nonspecific effect of fluorescence inhibition. A similar result was noted for compound RU-0102758, also shown in Fig. 6C. As shown in Supplementary Fig. S6, eight hits demonstrated activity in almost all of the DSB repair assays tested (depicted as black bar graphs), three hits demonstrated activity in two to three of the assays (depicted as dark gray bar graphs), while one hit only suppressed mNHEJ repair activity (depicted as light gray bar graphs). Collectively, these data suggest these compounds affect DSB repair activity, although their effects are diverse and warrant further study.

In addition, we tested the effects of our hits on the repair of IR-induced DSBs. DSB repair proteins form discrete foci at DNA damage sites after treatment with IR, which can be visualized by immunofluorescence microscopy. Such foci patterns can be used as markers for DSB repair in cultured cells (29, 30). Importantly, such foci-based assays represent an orthogonal secondary assay that would further support the functional activity of our identified hits as DSB repair inhibitors. We also reasoned that, as with the panel of GFP-based DSB repair assays, these foci-based studies could provide additional insights into the mechanisms by which the identified hits regulate DSB repair. To this end, we developed optimized protocols to detect IR-induced foci formation by a wide range of DNA-damage response and repair proteins, including phosphorylated DNA-PKcs (on threonine 2609 and serine 2056; T2609 and S2056, respectively), BRCA1, phosphorylated Chk2 (threonine 68), phosphorylated H2AX (γH2AX; on serine 139), and 53BP1. As discussed earlier, DNA-PK is a key cNHEJ factor that is recruited shortly after Ku70/80 binding to DSB ends, which then facilitates end processing and ligation of the DNA ends (13). Phosphorylation of T2609 and S2056 on DNA-PKcs promotes end processing (55) and DSB ligation (56), respectively, and there are well-established, commercially available antibodies specific to these two sites. Also mentioned earlier, BRCA1 is a key HR protein that binds to DSBs early in the DNA-damage response and competes with NHEJ factors to promote HR (57). Chk2 is an important kinase that is phosphorylated in response to DSBs created by IR, and which activates BRCA1 and several other key DNA-damage response mediators (58). Serine 139 phosphorylation on H2AX represents one of the earliest events in the cellular response to DSBs, and thus serves as a good control for DSB induction (59). 53BP1 serves as a molecular scaffold to recruit other key DSB repair proteins after H2AX phosphorylation, and recent studies suggest it plays a key role in DSB repair pathway choice (60). We tested the effects of each of our hits on foci formation by these proteins, 5 hours after a single 10 Gy IR dose in U2OS cells. In these assays, we tested compounds at 10 μmol/L concentrations in DMSO, and the drugs were added 1 hour before IR. The results for active hits are shown in Supplementary Fig. S7. None of the hits affected the γH2AX levels after IR, which is expected because few molecules have been described that can directly inhibit this early event in the DNA-damage response. However, each of the hits shown displayed aberrant foci formation for at least one of the targets that was studied. The results for compound RU-0097818 are shown in shown Fig. 6D, which are notable for substantial reductions in foci formation by phosphorylated DNA-PKcs, BRCA1, phosphorylated Chk2, and 53BP1. Importantly, this compound was also found to inhibit both mNHEJ and HR repair in the primary screen, as well as SSA and MMEJ in the GFP-based secondary assay studies. As mentioned above, we tested this compound at a 10 μmol/L concentration here, a dose that appears to inhibit all DSB repair pathways without affecting cell viability in the secondary GFP-based assays (see Supplementary Fig. S3). Of note, this drug has a slight preference for inhibition of mNHEJ over HR at lower doses (e.g., 1 μmol/L), and studies are ongoing to assess IR foci formation patterns under these conditions in our laboratory (data not shown). Taken together, these findings provide additional support that our identified hits are functionally active as DSB repair inhibitors, which was the goal of these particular experiments. Nonetheless, additional future studies are needed to elucidate the exact mechanism(s) by which these compounds inhibit DSB repair.

Assessment of novel DSB repair inhibitors as tumor cell radiosensitizers

Finally, we sought to test whether any of our identified hits could radiosensitize tumor cells *in vitro*. The inhibition of DSB repair is associated with increased sensitivity to IR (61), and thus the finding that our hits act as radiosensitizers would provide additional evidence, supporting their functional activity as DSB repair inhibitors. As discussed earlier, emerging evidence suggests that tumor cell radiosensitization via inhibition of DNA repair and damage checkpoints has great therapeutic potential for many solid tumors (5). Glioblastoma is a notable example, as despite aggressive surgical intervention followed by high doses of radiotherapy and chemotherapy, local recurrences are common (62). Given that we identified several known drugs in our primary screen, we reasoned that these hits could be rapidly translated into clinical testing if they also radiosensitized tumor cells. To this end, we tested each of our 16 hits in clonogenic survival assays, which are considered the "gold standard" for the assessment of IR response patterns *in vitro* (63, 64). We tested the parental U2OS cell line, and also an adult glioblastoma multiforme (GBM) cell line, T98G, in these experiments. In these assays, we tested compounds at 10 μmol/L concentrations in DMSO. Nine hits demonstrated radiosensitization in either or both cell lines at multiple IR doses, and representative data are shown in Fig. 7A. The observed radiosensitization was substantial, in the range of 1.4- to 2.6-fold for these compounds. Differences in IR-induced cell kill (without drugs) in these studies likely can be attributed to variations in the plating efficiencies and experimental conditions, because these compounds were tested in separate experiments. For example, RU-0084411 and RU-0000476 were tested as radiosensitizers in the same experiments, and they had similar levels of radiosensitization that correlated with similar effects in the secondary GFP-based reporter assays (see Supplementary Fig. S6). These experiments were also notable for no adverse effects on

Published OnlineFirst December 15, 2014; DOI: 10.1158/1535-7163.MCT-14-0765

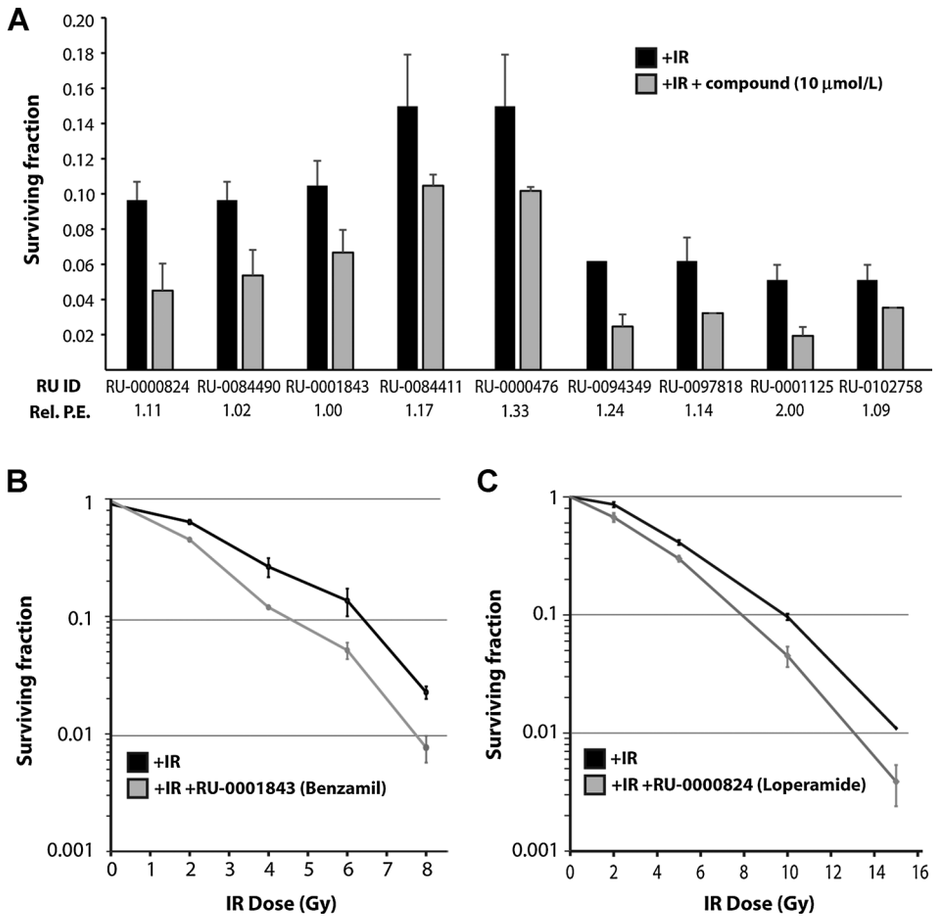

Figure 7.
Assessment of validated hits as tumor cell radiosensitizers *in vitro*. A, surviving fractions for the compounds with the most robust activity as radiosensitizers are shown for 8 Gy in U2OS cells (the first five compounds) and 10 Gy in T98G cells (the last four compounds). Error bars, SEMs from duplicate plating experiments. The relative plating efficiencies (P.E.s) between no IR and no IR with compound are shown for each hit, to highlight minimal effects on P.E. in the absence of IR. B and C, representative clonogenic survival assay curves are shown for two hits with substantial radiosensitization observed at all tested IR doses. Compounds were tested at 10 μmol/L concentrations.

plating efficiency in the presence of the compounds, which suggests a true synergistic interaction between IR and the molecules (65). Two known drugs, benzamil and loperamide, exhibited significant radiosensitization at each of the IR doses tested, and the complete clonogenic survival curves from representative experiments are shown in Figs. 7B and C, respectively. These data were also fitted to the linear quadratic model for IR survival (63, 64), which are presented in Supplementary Fig. S7B and S7C, respectively.

Finally, we sought to test whether mibefradil was active as a radiosensitizer in patient-derived primary tumor cell lines. Our group recently developed optimized and validated protocols to assess radio- and chemosensitization by test drugs in primary cell cultures, using a short-term growth delay assay (66). We have validated this assay in parallel clonogenic survival assays, and also with known radiosensitizers, using a collection of early-passage primary melanoma cell lines derived from patient tumors. As melanomas are known radioresistant tumors, there is great interest in radiosensitization for this disease, especially for melanoma brain metastases. We thus tested mibefradil as a radiosensitizer in this system, given that the platform was readily available in our laboratory, and also given the clinically relevant question. We used our previously established protocols in these experiments (66). As shown in Supplementary Fig. S7D, we detected substantial radiosensitization with mibefradil in primary melanoma cells. In these experiments, the mibefradil dose was reduced to 1 μmol/L, because initial studies in the absence of IR indicated that these primary cell cultures were substantially more sensitive to this drug compared with established cancer cell lines (data not shown). As shown in Supplementary Fig. S7D, the dose we tested for radiosensitization did not adversely affect cell viability (and possibly even increased the plating efficiency) in the absence of IR. Collectively, these data suggest that several of our validated hits inhibit DSB repair that is also associated with radiosensitization of tumor cells *in vitro*. Several of these compounds are either currently or previously FDA-approved drugs, which suggest the potential for rapidly translating them into clinical trials as radiosensitizers. Along these lines, we are now testing mibefradil as a glioma radiosensitizer in a clinical trial, which is discussed further below.

Discussion

Here, we present the design and execution of a cell-based, high-throughput screen for small molecule inhibitors of DSB repair. Specifically, we interrogated an approximately 20,000 compound library for molecules that alter either or both mNHEJ and HR repair activity, using a novel assay recently developed by our group. This study has revealed several interesting hits that were validated in a comprehensive panel of secondary DSB repair assays. Importantly, several of the compounds that we identified in this screen demonstrated tumor cell radiosensitivity *in vitro*.

Published OnlineFirst December 15, 2014; DOI: 10.1158/1535-7163.MCT-14-0765

Many novel structures were identified that potently inhibited DSB repair with minimal effects on cell viability. Furthermore, we identified several novel DSB repair inhibitors that are either known or previously FDA-approved drugs. These hits are of particular interest, because they may be repurposed as radiosensitizers for clinical use in the near future.

Our study is unique because it analyzes the effects of small molecules on two major DSB repair pathways simultaneously, while also assessing effects on cell viability in parallel. This approach permits one to rapidly exclude molecules that indirectly affect DSB repair via toxic effects, and it can immediately yield information on the selectivity of a given hit on a particular DSB repair pathway. In addition, the incorporation of orthogonal secondary assays to further interrogate DSB repair subpathways provides a key validation step to assess the functional significance of the identified hits. Shahar and colleagues (67) recently reported the results of a 96-well plate-based, DR-GFP screen of 1,200 approved drugs for novel HR modulators. These studies revealed three drugs that inhibited HR: spirolactone, aripiprazole, and hycanthone. Interestingly, spirolactone was found to sensitize cells to cisplatin, mitomycin C, and PARP inhibitors. Of note, this study also used a glucocorticoid receptor–based inducible I-Sce cleavage system, which we recently engineered further to create ddSceGR (27). This study also differed from our screen in that the drugs were continuously incubated for approximately 64 hours with the cells during the screen, and a higher screening concentration was used (20 μmol/L). We incubated cells with compounds at 10 μmol/L concentrations for only 24 hours to minimize potentially confounding effects on viability. The three drug hits identified in this previous study were observed to inhibit HR repair in our screen, although they were below our defined threshold for significance. This could be, in part, attributed to our lower drug screening concentrations and shorter incubation times. Several other small molecule screens for DSB repair inhibitors have been reported previously, although most of these studies consisted of *in vitro* screens focused on disrupting the activity of Rad51 (68–71). To our knowledge, there have been no published cell-based screens focused on identifying small molecules that block NHEJ repair pathways.

We identified several novel molecules that inhibited mNHEJ and/or HR repair to nearly undetectable levels in our screen. Remarkably, many of these compounds had minimal effects on cell viability, even at the highest concentrations tested. We were also surprised to find compounds that specifically blocked unique and unexpected combinations of HR, SSA, and the NHEJ subpathways. For example, several hits specifically blocked mNHEJ repair without affecting MMEJ, such as RU-000824 (loperamide) and RU-0005520. As noted earlier, our mNHEJ assay measures any mNHEJ repair events, whereas the MMEJ assay specifically measures NHEJ repair events that use a single 8 bp flanking microhomology sequence. Further studies are needed to understand the mechanisms underlying these differential results. Recent studies suggest that mNHEJ-related pathways are used to repair DSBs at collapsed forks in S-phase (34), and that these pathways may be suppressed in quiescent cells (27, 72). It is thus tempting to speculate that pharmacologic inhibition of mNHEJ will preferentially radiosensitize actively replicating tumor cells over G_0–G_1-arrested normal tissues.

Our IR foci–based secondary assays revealed that each hit altered the DNA-damage response, although further studies are needed to understand the significance of these changes. In particular, it will be critical to study these foci patterns over multiple time points to assess kinetics, which likely will yield further insights into the effects of our hits on DSB repair processes. For example, our laboratory has recently found that most small molecule DNA-PKcs inhibitors do not suppress the levels of IR-induced phosphorylated DNA-PKcs foci formation; rather, they induce a persistence of these foci at DSBs after IR (Bindra laboratory; unpublished results). Furthermore, the study of foci formation patterns for other key DNA repair proteins in the presence of our hits will also be important to gain additional mechanistic insights. It should also be noted that we excluded several hits that significantly reduced mNHEJ and/or HR repair, but which also substantially reduced cell viability (i.e., >50% reductions in cell numbers). One notable example was helenine, which reduced mNHEJ and HR repair activity to 20% and 6%, respectively, although cell viability was also reduced to 20% (relative to DMSO-treated cells). Helenine is an antiviral drug that has been used therapeutically previously, but it is not in clinical use currently (73). These hits could be of great interest, because it is possible that the effects on viability are not related to the DSB repair phenotype(s), especially because we measured cell numbers at 96 hours. For example, cell toxicity could occur 48 to 96 hours after compound exposure, which would not be expected to affect the DSB repair processes occurring during the initial 0 to 48 hours phase of the assay protocol. Studies are ongoing in our laboratory to evaluate these possibilities.

As presented in Supplementary Fig. S5A, we confirmed that incubation with known small molecule DNA-PKcs inhibitors substantially altered DSB repair pathway utilization in U2OS cells. An overall trend for increased activity in multiple reporter assays was observed, consistent with inhibition of cNHEJ repair leading to upregulated HR, SSA, and other noncanonical NHEJ repair pathways (27, 53, 54). However, we found it surprising that the two DNA-PKcs inhibitors we tested demonstrated unique, and in some cases unexpected, differences in reporter assay phenotypes. For example, the DNA-PKcs inhibitor, DNA-PK V, predominantly induced an increase in SSA repair activity (74). We have confirmed previously that these drugs induce substantial radiosensitivity in U2OS cells at the doses tested here, which confirms the functional activity of both agents as DSB repair inhibitors (data not shown; refs. 27). These results suggest subtle differences in DNA-PKcs inhibitors on overall DSB repair, which warrants further study. Similarly, we were surprised to find that inhibitors of both topoisomerase I and II had profound effects on multiple DSB repair pathways (Supplementary Fig. S5B). These effects were apparent at doses of drug well below that observed affecting cell viability (e.g., 1 μmol/L for etoposide; data not shown). Furthermore, we found that multiple drugs in these classes repressed DSB repair in the EJ-DRs assay (including camptothecin, irinotecan, and teniposide; data not shown).

Finally, the findings that multiple known FDA-approved drugs have activity as DSB repair inhibitors and tumor cell radiosensitizers raise the possibility that these agents can be readily tested in clinical trials as radiosensitizers in the near future. As discussed earlier, GBM tumors would be an ideal target to test such agents, because they are exquisitely radioresistant tumors, and local recurrence is the predominant mode of failure for these tumors (62). Drugs in our hit-list, such as mibefradil, pimozide, and AMN082, are of particular interest for the treatment of brain tumors, because they are known to penetrate the blood brain

Published OnlineFirst December 15, 2014; DOI: 10.1158/1535-7163.MCT-14-0765

barrier (75–77). Intriguingly, mibefradil has been shown to synergize with both temozolomide chemotherapy and IR, both *in vitro* in glioma cell lines, and *in vivo* in mouse GBM xenografts (78–80). These findings are consistent with our observations in this study that mibefradil inhibits mNHEJ repair and radiosensitizes glioma cells. As described above, we believe there is an inherent therapeutic index to targeting mNHEJ, which may allow for selective glioma tumor cell radiosensitization with mibefradil. On the basis of the data presented here and recently published by our collaborators (78–80), we recently initiated a phase I clinical trial at Yale, testing mibefradil as a glioma radiosensitizer (Trial#NCT02202993). Work is ongoing in our laboratory to elucidate the exact mechanism(s) by which mibefradil inhibits mNHEJ repair. Similar efforts are underway for pimozide at our institution, which also inhibits DSB repair and leads to substantial tumor cell radiosensitivity (data not shown). These efforts highlight the potential utility of repurposing known drugs as radiosensitizers in clinical trials.

In summary, we have identified a small collection of novel compounds in a unique cell-based screen that inhibit key DSB repair pathways, a selection of which are known drugs and which radiosensitize tumor cells *in vitro*. In future studies, we will interrogate a larger compound library (e.g., >100K molecules) for additional molecules using our screening platform. Studies are also under way to further elucidate the mechanisms of action by which the compounds identified in this screen regulate DSB repair. Selected hits will also be tested for radiosensitization using xenograft tumors grown in mice, to confirm that they have activity *in vivo*. For the known drugs identified in this study, efforts are now focused on repurposing them as radiosensitizers for radioresistant tumors such as high-grade gliomas. NCT02202993 is one such example, in which we are testing one of the hits from this screen, mibefradil, as a radiosensitizer in patients with recurrent GBM.

Disclosure of Potential Conflicts of Interest

No potential conflicts of interest were disclosed.

Authors' Contributions

Conception and design: M. Jasin, S.N. Powell, R.S. Bindra
Development of methodology: A.G. Goglia, D. Shahbazian, J.A. Wilshire, J.F. Glickman, R.S. Bindra
Acquisition of data (provided animals, acquired and managed patients, provided facilities, etc.): A.G. Goglia, A.N. Luz, D. Shahbazian, A.F. Salem, R.K. Sundaram, J. Chiaravalli, P.J. Hendrikx, J.A. Wilshire, H. Kluger, J.F. Glickman, R.S. Bindra
Analysis and interpretation of data (e.g., statistical analysis, biostatistics, computational analysis): A.G. Goglia, A.N. Luz, A.F. Salem, J. Chiaravalli, P.J. Hendrikx, J.F. Glickman, S.N. Powell, R.S. Bindra
Writing, review, and/or revision of the manuscript: A.G. Goglia, A.N. Luz, J. Chiaravalli, J.F. Glickman, S.N. Powell, R.S. Bindra
Administrative, technical, or material support (i.e., reporting or organizing data, constructing databases): R. Delsite, A.N. Luz, P.J. Hendrikx, J.A. Wilshire, H. Kluger, J.F. Glickman
Study supervision: S.N. Powell

Acknowledgments

The authors thank Dr. Jeremy Stark for providing U2OS cell lines with integrated GFP-based reporters to measure total NHEJ, SSA, and MMEJ repair activity.

The costs of publication of this article were defrayed in part by the payment of page charges. This article must therefore be hereby marked advertisement in accordance with 18 U.S.C. Section 1734 solely to indicate this fact.

Received September 9, 2014; revised November 17, 2014; accepted November 19, 2014; published OnlineFirst December 15, 2014.

References

1. Smith-Roe SL, Patel SS, Zhou Y, Simpson DA, Rao S, Ibrahim JG, et al. Separation of intra-S checkpoint protein contributions to DNA replication fork protection and genomic stability in normal human fibroblasts. Cell Cycle 2013;12:332–45.
2. Kaufmann WK, Anderson CW. Compensation, crosstalk and sequestering: the currency of checkpoints in cancer. Cell Cycle 2013;12:1163–4.
3. Morandell S, Yaffe MB. Exploiting synthetic lethal interactions between DNA damage signaling, checkpoint control, and p53 for targeted cancer therapy. Prog Mol Biol Transl Sci 2012;110:289–314.
4. Kaufmann WK. Cell cycle checkpoints and DNA repair preserve the stability of the human genome. Cancer Metastasis Rev 1995;14:31–41.
5. Thoms J, Bristow RG. DNA repair targeting and radiotherapy: a focus on the therapeutic ratio. Semin Radiat Oncol 2010;20:217–22.
6. Senra JM, Telfer BA, Cherry KE, McCrudden CM, Hirst DG, O'Connor MJ, et al. Inhibition of PARP-1 by olaparib (AZD2281) increases the radiosensitivity of a lung tumor xenograft. Mol Cancer Ther 2011;10:1949–58.
7. Morgan MA, Parsels LA, Zhao L, Parsels JD, Davis MA, Hassan MC, et al. Mechanism of radiosensitization by the Chk1/2 inhibitor AZD7762 involves abrogation of the G_2 checkpoint and inhibition of homologous recombinational DNA repair. Cancer Res 2010;70:4972–81.
8. Tavecchio M, Munck JM, Cano C, Newell DR, Curtin NJ. Further characterisation of the cellular activity of the DNA-PK inhibitor, NU7441, reveals potential cross-talk with homologous recombination. Cancer Chemother Pharmacol 2012;69:155–64.
9. Schenone M, Dancik V, Wagner BK, Clemons PA. Target identification and mechanism of action in chemical biology and drug discovery. Nat Chem Biol 2013;9:232–40.
10. Ciccia A, Elledge SJ. The DNA damage response: making it safe to play with knives. Mol Cell 2010;40:179–204.
11. Shibata A, Conrad S, Birraux J, Geuting V, Barton O, Ismail A, et al. Factors determining DNA double-strand break repair pathway choice in G_2 phase. EMBO J 2011;30:1079–92.
12. Frit P, Barboule N, Yuan Y, Gomez D, Calsou P. Alternative end-joining pathway(s): bricolage at DNA breaks. DNA Repair 2014;17:81–97.
13. Lieber MR. The mechanism of human nonhomologous DNA end joining. J Biol Chem 2008;283:1–5.
14. Corneo B, Wendland RL, Deriano L, Cui X, Klein IA, Wong SY, et al. Rag mutations reveal robust alternative end joining. Nature 2007;449:483–6.
15. Guirouilh-Barbat J, Rass E, Plo I, Bertrand P, Lopez BS. Defects in XRCC4 and KU80 differentially affect the joining of distal nonhomologous ends. Proc Natl Acad Sci U S A 2007;104:20902–7.
16. Soulas-Sprauel P, Le Guyader G, Rivera-Munoz P, Abramowski V, Olivier-Martin C, Goujet-Zalc C, et al. Role for DNA repair factor XRCC4 in immunoglobulin class switch recombination. J Exp Med 2007;204:1717–27.
17. Yan CT, Boboila C, Souza EK, Franco S, Hickernell TR, Murphy M, et al. IgH class switching and translocations use a robust non-classical end-joining pathway. Nature 2007;449:478–82.
18. Xie A, Kwok A, Scully R. Role of mammalian Mre11 in classical and alternative nonhomologous end joining. Nat Struct Mol Biol 2009;16:814–8.
19. Wang M, Wu W, Wu W, Rosidi B, Zhang L, Wang H, et al. PARP-1 and Ku compete for repair of DNA double strand breaks by distinct NHEJ pathways. Nucleic Acids Res 2006;34:6170–82.
20. Saribasak H, Maul RW, Cao Z, McClure RL, Yang W, McNeill DR, et al. XRCC1 suppresses somatic hypermutation and promotes alternative nonhomologous end joining in Igh genes. J Exp Med 2011;208:2209–16.
21. Caldecott KW, Tucker JD, Stanker LH, Thompson LH. Characterization of the XRCC1-DNA ligase III complex *in vitro* and its absence from mutant hamster cells. Nucleic Acids Res 1995;23:4836–43.

22. Han L, Mao W, Yu K. X-ray repair cross-complementing protein 1 (XRCC1) deficiency enhances class switch recombination and is permissive for alternative end joining. Proc Natl Acad Sci U S A 2012;109:4604–8.
23. Boboila C, Oksenych V, Gostissa M, Wang JH, Zha S, Zhang Y, et al. Robust chromosomal DNA repair via alternative end-joining in the absence of X-ray repair cross-complementing protein 1 (XRCC1). Proc Natl Acad Sci U S A 2012;109:2473–8.
24. Simsek D, Furda A, Gao Y, Artus J, Brunet E, Hadjantonakis AK, et al. Crucial role for DNA ligase III in mitochondria but not in Xrcc1-dependent repair. Nature 2011;471:245–8.
25. Symington LS, Gautier J. Double-strand break end resection and repair pathway choice. Annu Rev Genet 2011;45:247–71.
26. Lee K, Lee SE. *Saccharomyces cerevisiae* Sae2- and Tel1-dependent single-strand DNA formation at DNA break promotes microhomology-mediated end joining. Genetics 2007;176:2003–14.
27. Bindra RS, Goglia AG, Jasin M, Powell SN. Development of an assay to measure mutagenic non-homologous end-joining repair activity in mammalian cells. Nucleic Acids Res 2013;41:e115.
28. Lin FL, Sperle K, Sternberg N. Model for homologous recombination during transfer of DNA into mouse L cells: role for DNA ends in the recombination process. Mol Cell Biol 1984;4:1020–34.
29. Martin NT, Nahas SA, Tunuguntla R, Fike F, Gatti RA. Assessing `radiosensitivity' with kinetic profiles of gamma-H2AX, 53BP1 and BRCA1 foci. Radiother Oncol 2011;101:35–8.
30. Banath JP, Macphail SH, Olive PL. Radiation sensitivity, H2AX phosphorylation, and kinetics of repair of DNA strand breaks in irradiated cervical cancer cell lines. Cancer Res 2004;64:7144–9.
31. Kent CR, Eady JJ, Ross GM, Steel GG. The comet moment as a measure of DNA damage in the comet assay. Int J Radiat Biol 1995;67:655–60.
32. Weingeist DM, Ge J, Wood DK, Mutamba JT, Huang Q, Rowland EA, et al. Single-cell microarray enables high-throughput evaluation of DNA double-strand breaks and DNA repair inhibitors. Cell Cycle 2013;12:907–15.
33. Pierce AJ, Johnson RD, Thompson LH, Jasin M. XRCC3 promotes homology-directed repair of DNA damage in mammalian cells. Genes Dev 1999;13:2633–8.
34. Truong LN, Li Y, Shi LZ, Hwang PY, He J, Wang H, et al. Microhomology-mediated end joining and homologous recombination share the initial end resection step to repair DNA double-strand breaks in mammalian cells. Proc Natl Acad Sci U S A 2013;110:7720–5.
35. Bennardo N, Cheng A, Huang N, Stark JM. Alternative-NHEJ is a mechanistically distinct pathway of mammalian chromosome break repair. PLoS Genet 2008;4:e1000110.
36. Bennardo N, Stark JM. ATM limits incorrect end utilization during non-homologous end joining of multiple chromosome breaks. PLoS Genet 2010;6:e1001194.
37. Willers H, Husson J, Lee LW, Hubbe P, Gazemeier F, Powell SN, et al. Distinct mechanisms of nonhomologous end joining in the repair of site-directed chromosomal breaks with noncomplementary and complementary ends. Radiat Res 2006;166:567–74.
38. Hartlerode A, Odate S, Shim I, Brown J, Scully R. Cell cycle–dependent induction of homologous recombination by a tightly regulated I-SceI fusion protein. PLoS ONE 2011;6:e16501.
39. Lundholt BK, Scudder KM, Pagliaro L. A simple technique for reducing edge effect in cell-based assays. J Biomol Screen 2003;8:566–70.
40. Black CB, Duensing TD, Trinkle LS, Dunlay RT. Cell-based screening using high-throughput flow cytometry. Assay Drug Dev Technol 2011;9:13–20.
41. Munshi A, Hobbs M, Meyn RE. Clonogenic cell survival assay. Methods Mol Med 2005;110:21–8.
42. Soutoglou E, Dorn JF, Sengupta K, Jasin M, Nussenzweig A, Ried T, et al. Positional stability of single double-strand breaks in mammalian cells. Nat Cell Biol 2007;9:675–82.
43. Torrance CJ, Agrawal V, Vogelstein B, Kinzler KW. Use of isogenic human cancer cells for high-throughput screening and drug discovery. Nat Biotechnol 2001;19:940–5.
44. Zhang JH, Chung TD, Oldenburg KR. A simple statistical parameter for use in evaluation and validation of high throughput screening assays. J Biomol Screen 1999;4:67–73.
45. Dupre A, Boyer-Chatenet L, Sattler RM, Modi AP, Lee JH, Nicolette ML, et al. A forward chemical genetic screen reveals an inhibitor of the Mre11–Rad50–Nbs1 complex. Nat Chem Biol 2008;4:119–25.
46. Korn K, Krausz E. Cell-based high-content screening of small-molecule libraries. Curr Opin Chem Biol 2007;11:503–10.
47. Fattah F, Lee EH, Weisensel N, Wang Y, Lichter N, Hendrickson EA. Ku regulates the non-homologous end joining pathway choice of DNA double-strand break repair in human somatic cells. PLoS Genet 2010;6:e1000855.
48. Baell JB, Holloway GA. New substructure filters for removal of pan assay interference compounds (PAINS) from screening libraries and for their exclusion in bioassays. J Med Chem 2010;53:2719–40.
49. Shi LM, Fan Y, Lee JK, Waltham M, Andrews DT, Scherf U, et al. Mining and visualizing large anticancer drug discovery databases. J Chem Inf Comput Sci 2000;40:367–79.
50. Mansour WY, Rhein T, Dahm-Daphi J. The alternative end-joining pathway for repair of DNA double-strand breaks requires PARP1 but is not dependent upon microhomologies. Nucleic Acids Res 2010;38:6065–77.
51. Mansour WY, Schumacher S, Rosskopf R, Rhein T, Schmidt-Petersen F, Gatzemeier F, et al. Hierarchy of nonhomologous end-joining, single-strand annealing and gene conversion at site-directed DNA double-strand breaks. Nucleic Acids Res 2008;36:4088–98.
52. Schulte-Uentrop L, El-Awady RA, Schliecker L, Willers H, Dahm-Daphi J. Distinct roles of XRCC4 and Ku80 in non-homologous end-joining of endonuclease- and ionizing radiation-induced DNA double-strand breaks. Nucleic Acids Res 2008;36:2561–9.
53. Allen C, Halbrook J, Nickoloff JA. Interactive competition between homologous recombination and non-homologous end joining. Mol Cancer Res 2003;1:913–20.
54. Convery E, Shin EK, Ding Q, Wang W, Douglas P, Davis LS, et al. Inhibition of homologous recombination by variants of the catalytic subunit of the DNA-dependent protein kinase (DNA-PKcs). Proc Natl Acad Sci U S A 2005;102:1345–50.
55. Meek K, Douglas P, Cui X, Ding Q, Lees-Miller SP. trans Autophosphorylation at DNA-dependent protein kinase's two major autophosphorylation site clusters facilitates end processing but not end joining. Mol Cell Biol 2007;27:3881–90.
56. Cui X, Yu Y, Gupta S, Cho YM, Lees-Miller SP, Meek K. Autophosphorylation of DNA-dependent protein kinase regulates DNA end processing and may also alter double-strand break repair pathway choice. Mol Cell Biol 2005;25:10842–52.
57. Bunting SF, Callen E, Wong N, Chen HT, Polato F, Gunn A, et al. 53BP1 inhibits homologous recombination in Brca1-deficient cells by blocking resection of DNA breaks. Cell 2010;141:243–54.
58. Matsuoka S, Huang M, Elledge SJ. Linkage of ATM to cell cycle regulation by the Chk2 protein kinase. Science 1998;282:1893–7.
59. Rogakou EP, Pilch DR, Orr AH, Ivanova VS, Bonner WM. DNA double-stranded breaks induce histone H2AX phosphorylation on serine 139. J Biol Chem 1998;273:5858–68.
60. Panier S, Boulton SJ. Double-strand break repair: 53BP1 comes into focus. Nat Rev Mol Cell Biol 2014;15:7–18.
61. Pollard JM, Gatti RA. Clinical radiation sensitivity with DNA repair disorders: an overview. Int J Radiat Oncol Biol Phys 2009;74:1323–31.
62. Laperriere N, Zuraw L, Cairncross G. Radiotherapy for newly diagnosed malignant glioma in adults: a systematic review. Radiother Oncol 2002;64:259–73.
63. Puck TT, Marcus PI. Action of x-rays on mammalian cells. J Exp Med 1956;103:653–66.
64. Sumantran VN. Cellular chemosensitivity assays: an overview. Methods Mol Biol 2011;731:219–36.
65. Steel GG. The search for therapeutic gain in the combination of radiotherapy and chemotherapy. Radiother Oncol 1988;11:31–53.
66. Shahbazian D, Bindra RS, Kluger HM, Glazer PM. Radiation sensitivity and sensitization in melanoma. Pigment Cell Melanoma Research 2013;26:928–30.
67. Shahar OD, Kalousi A, Eini L, Fisher B, Weiss A, Darr J, et al. A high-throughput chemical screen with FDA approved drugs reveals that the antihypertensive drug Spironolactone impairs cancer cell survival by inhibiting homology directed repair. Nucleic Acids Res 2014;42:5689–701.
68. Jayathilaka K, Sheridan SD, Bold TD, Bochenska K, Logan HL, Weichselbaum RR, et al. A chemical compound that stimulates the human homologous recombination protein RAD51. Proc Natl Acad Sci U S A 2008;105:15848–53.

Published OnlineFirst December 15, 2014; DOI: 10.1158/1535-7163.MCT-14-0765

69. Budke B, Logan HL, Kalin JH, Zelivianskaia AS, Cameron McGuire W, Miller LL, et al. RI-1: a chemical inhibitor of RAD51 that disrupts homologous recombination in human cells. Nucleic Acids Res 2012;40:7347–57.
70. Huang F, Mazina OM, Zentner IJ, Cocklin S, Mazin AV. Inhibition of homologous recombination in human cells by targeting RAD51 recombinase. J Med Chem 2012;55:3011–20.
71. Huang F, Motlekar NA, Burgwin CM, Napper AD, Diamond SL, Mazin AV. Identification of specific inhibitors of human RAD51 recombinase using high-throughput screening. ACS Chem Biol 2011;6:628–35.
72. Singh SK, Wu W, Zhang L, Klammer H, Wang M, Iliakis G. Widespread dependence of backup NHEJ on growth state: ramifications for the use of DNA-PK inhibitors. Int J Radiat Oncol Biol Phys 2011;79:540–8.
73. Shope RE. An antiviral substance from Penicillium funiculosum. VII. An attempt to determine whether the material responsible for the antipassive immunity effect exhibited by mice injected with helenine is an interferon. J Exp Med 1966;124:915–9.
74. Knight ZA, Chiang GG, Alaimo PJ, Kenski DM, Ho CB, Coan K, et al. Isoform-specific phosphoinositide 3-kinase inhibitors from an arylmorpholine scaffold. Bioorg Med Chem 2004;12:4749–59.
75. Sukoff Rizzo SJ, Leonard SK, Gilbert A, Dollings P, Smith DL, Zhang MY, et al. The metabotropic glutamate receptor 7 allosteric modulator AMN082: a monoaminergic agent in disguise? J Pharmacol Exp Ther 2011;338:345–52.
76. Lacinova L. Pharmacology of recombinant low-voltage activated calcium channels. Curr Drug Target CNS Neurol Disord 2004;3:105–11.
77. Egolf A, Coffey BJ. Current pharmacotherapeutic approaches for the treatment of Tourette syndrome. Drugs Today 2014;50:159–79.
78. Keir ST, Friedman HS, Reardon DA, Bigner DD, Gray LA. Mibefradil, a novel therapy for glioblastoma multiforme: cell cycle synchronization and interlaced therapy in a murine model. J Neurooncol 2013;111:97–102.
79. Sheehan JP, Xu Z, Popp B, Kowalski L, Schlesinger D. Inhibition of glioblastoma and enhancement of survival via the use of mibefradil in conjunction with radiosurgery. J Neurosurg 2013;118:830–7.
80. Valerie NC, Dziegielewska B, Hosing AS, Augustin E, Gray LS, Brautigan DL, et al. Inhibition of T-type calcium channels disrupts Akt signaling and promotes apoptosis in glioblastoma cells. Biochem Pharmacol 2013;85:888–97.

Published OnlineFirst December 15, 2014; DOI: 10.1158/1535-7163.MCT-14-0765

Molecular Cancer Therapeutics

Identification of Novel Radiosensitizers in a High-Throughput, Cell-Based Screen for DSB Repair Inhibitors

Alexander G. Goglia, Robert Delsite, Antonio N. Luz, et al.

Mol Cancer Ther 2015;14:326-342. Published OnlineFirst December 15, 2014.